Deltares

Simulating Coastal Morphodynamics with Delft3D: case study Egmond aan Zee

Alessio Giardino
Jebbe van der Werf
Maarten van Ormondt

1200635-005

Deltares

Title
Simulating Coastal Morphodynamics with Delft3d: case study Egmond aan Zee

Client	Project	Pages
Waterdienst	1200635-005	72

Keywords
Morphodynamics modelling, Delft3D improvements, nourishments.

Summary
The numerical modelling of shoreface nourishments and bar dynamics is one of the most challenging tasks in computational morphodynamics. This is mostly related with the complexity of the physical processes involved, in particular in the cross-shore direction. Walstra et al. (2008) investigated the possibility of representing bar dynamics and nourishment scenarios by means of the Delft3D code. Although they were able to simulate the main cross-shore and longshore dynamics, they pointed out one significant limitation in the calculations: the formation of regular bedforms, growing out of control during the simulations and limiting the possibility of running long term computations.

In the framework of this work, a number of modifications to the Delf3D code were implemented and tested to improve the morphodynamics results. The main modifications applied to the code consist in the calculation of the bed shear stress, the numerical scheme for computing suspended sediment transport, and the numerical scheme of short wave energy and roller energy propagation near structures and hard points. Moreover, the module carrying out the Delft-3D calculation in Quasi-3D mode was modified, and a beach and dune module was included in the code. However, these last two modifications were not tested in this study.

Results obtained with the standard and modified Delft3D versions were compared for different angles of wave attack and at different instants in the tidal cycle. Moreover, the behaviour of a nourishment scenario was simulated with the two versions of the code. Modelling results show an increase in the longshore currents, mainly resulting from the new method used for computing bed shear stress. This reflects into a smoother bathymetry where the bed instabilities observed by Walstra et al. (2008) are less pronounced. However, further work is necessary to validate these computations by comparing them with hydrodynamic, wave and morphodynamic measurements.

Version	Date	Author	Initials	Review	Initials	Approval	Initials
1.0	Dec. 2009	Dr. Ir. Alessio Giardino		Prof. Dr. Ir. Leo van Rijn		Ir. T.Schilperoort	
2.0	Jan. 2010	Dr. Ir. Jebbe van der Werf					
		Ir. Maarten van Ormondt					

State
final

Contents

1 Introduction

1.1 Background

In The Netherlands, the coastline is maintained by means of sand nourishments. Since the late 1990's most of the sand is placed under water on the shore face, instead of on the beach. This is reflected in the current guidelines for nourishments, which can be summarized very generally as "if possible nourish on the shore face, if necessary nourish on the beach".

The design of effective and efficient shore face nourishments requires insight into the long term (years) morphodynamic behaviour of the nourished and adjacent coastal area, and the effect of design variables (e.g. nourishment volume) on this behaviour. The morphological modelling system Delft3D is (potentially) a powerful tool to investigate this. This requires that Delft3D is able to reliably simulate coastal morphodynamics on a temporal scale of years and a spatial scale of km's, respectively corresponding to the lifetime and the affected area of a nourishment.

Walstra et al. (2004) investigated the effects of various nourishment designs on the nearshore morphology using Delft3D, both in profile (two-dimensional vertical, 2DV) and in area (three-dimensional, 3D) mode. They used a longshore uniform bathymetry representative of the coastal town of Egmond, and compared the morphology after 1 year of simulation of 7 different nourishments (with different depths, volumes and alongshore lengths) to the unnourished situation. Their main conclusions were that (i) the effects of all nourishment designs are clearly noticeable after one year, (ii) the alongshore development of the nourishment is dominated by diffusive processes, (iii) the construction height does not seem to affect the nourishment lifetime, (iv) lifetime of the nourishment seems to be primarily governed by the total volume, and (v) Delft3D is able to make qualitatively realistic predictions of the cross-shore profile development.

One of these nourishment designs was studied again by Walstra et al. (2008) using a very similar 2DV and 3D model. This study used the latest updates to the sediment transport relation of Van Rijn 2007 (a,b,c) and the parameters settings were different from those used by Walstra et al. (2004). Conclusions regarding the morphodynamic behaviour of the nourishment were similar to those presented by Walstra et al. (2004). The area model was also used to study the shoreface nourishment that was carried out at Egmond in 2004. The area model was unable to make predictions on longer time scales (years) due to the unlimited development of rip-like instabilities along the shoreline, which after one month of simulation affected the entire surf zone. These instabilities were considered to be unrealistic and due to, among other things, an underestimation of the wave-driven longshore currents close to the shore.

1.2 Objectives

Our general research objective is to improve the capability of Delft3D to predict the morphodynamic impact of a shoreface nourishment on a temporal scale of years. More specifically, we will address the following research questions:

1) Which are the wave conditions responsible to the main growth of the bottom instabilities
2) How can Delft3D be adjusted to avoide the unlimited growth of rip-like instabilities?
3) Will the adjustments allow to run morphodynamic simulations for long time periods (time scale of years)?
4) What is the morphodynamic impact of a shoreface nourishment after one year according to the standard and adjusted Delft3D modelling system, and how well does this qualitatively compare to field observations?

1.3 Outline of the report

These research questions will be addressed by computations with a 3D model of a schematized Egmond case, similar to those used in Walstra et al (2004, 2008). The model set-up is described in Chapter 2. Besides the description of the standard Delft3D model, a number of modifications to the code are proposed, which would possible improve the results shown by previous studies. In Chapter 3 the sensitivity of the standard and modified Delft3D versions of the code to the angle of wave attack is tested. These tests aim to identify the wave conditions which possibly lead to restrictions in the morphodynamic computation. The two versions of the code are then applied in order to carry out a morphodynamic simulation for one specific nourishment scenario (Chapter 4). The overall conclusions and recommendations for further research are presented in Chapter 5.

2 Model set-up

2.1 Introduction

Within the framework of the Project Kustlijnzorg 2008, considerable effort was put into the development, validation and application of a morphodynamic model capable of representing the nearshore processes and their response to different nourishment scenarios. The wide range of data and previous studies carried out at Egmond aan Zee (The Netherlands) allowed for a comparison and discussion of the simulated results (Walstra et al., 2004; Walstra et al., 2008).

The Delft3D software was used to carry out the numerical simulations. The modelling system includes a module to carry out the hydrodynamic computation (Delft3D-FLOW), a module to compute the wave propagation (Delft3D-WAVE), and a module to compute the sediment transport and morphodynamic evolution under the combined action of currents and waves (Delft3D-SED).

In this Chapter, the model set-up is discussed. At first, the study area is described (Section 2.2). In Section 2.3 an overview of the numerical modules is given. The computational grids used to solve the wave, hydrodynamics, sediment computation are presented in Section 2.4. The boundary conditions used to drive the numerical simulations are described in Section 2.5.

2.2 Study area

Egmond aan Zee is located in the central part of the Dutch coast (Figure 2.1).

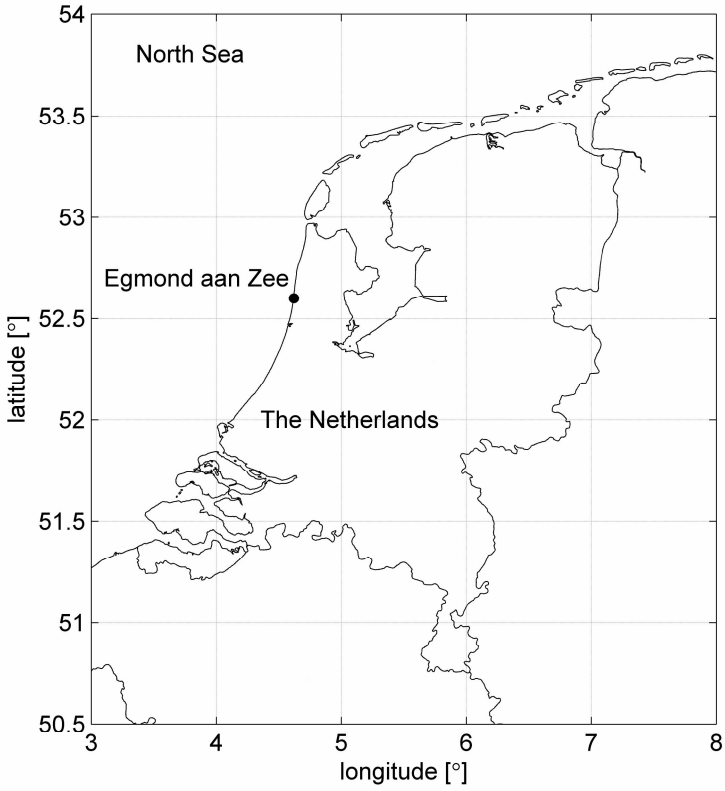

Figure 2.1 Geographical location of Egmond aan Zee (The Netherlands).

Much attention has been given in recent years to this site, due to the short lifetime duration of beach nourishments. In order to improve the coastal stability, and to assist the beach nourishments, two shoreface nourishment were applied in 1999 and 2004 (Van Duin et al., 2004, Walstra et al., 2008).

From a hydrodynamic point of view, Egmond aan Zee is characterized by a lower mesotidal regime, with a mean tidal range varying from 1.2 m at neap tide and 2.1 m at spring tide. Tidal currents are asymmetric with a stronger component towards the North. The peak longshore flood velocities (north directed) are about 0.5 m/s.
Wave height is characterized by a high seasonality with a mean wave height of about 1 m during the summer months and ranging between 1.5 – 1.7 m in the winter periods. More frequent waves come from the South West.
The coastal profile is characterized by a three-bar system: two breaker bars in the surf zone and a swash bar. The outer bar is more pronounced, being characterized by a crest at -3 m below MSL (Mean Sea Level). This bar is located at 500 m offshore. A through with a depth equal to -5 m below MSL separates the outer bar from the inner bar. The inner bar crest is located 200 m offshore and its crest is located at 1 m below MSL. Between the inner bar and the swash bar is a through, with a water depth equal to 2 m below MSL. The cross shore slope amounts to 1:100 (Van Duin et al., 2004).

On a large longshore scale the coastline at Egmond might appear uniform. However, at smaller scale the presence of irregularities due to rhythmic and quasi-rhytmic feautures are prove of a high cross and longshore complexity. Moreover, these features are characterized by movements in the two directions (long and cross shore), with a migration rate dependent on the combined current and wave conditions (Short, 1992).

The area is characterized by medium well-sorted sands (0.25 to 0.5 mm), although in the trough between the inner and outer bars, the sand is coarser (> 0.5 mm) and has a moderate sorting (Elias et al., 2000).

2.3 The models

Numerical simulations were carried out by means of the Delft3D software. In particular, the hydrodynamic and sediment transport module Delft3D-FLOW, and the wave module Delft3D-WAVE were used (Lesser et al., 2004). A scheme of a morphodynamic simulation is shown in Figure 2.2. The Delft3D-FLOW and Delft-3D-WAVE exchange information by means of a on-line coupling. In particular, every 10' (coupling time step) a new flow field (water level h and depth averaged currents u and v) is supplied from the flow model to the wave model. Delft3D-WAVE solves the balance equation of wave action density in the modelled domain and provides to Delft3D-FLOW peak wave frequency (fp) and mean wave direction (Θ). This information is used in the roller model of Delft3D-FLOW to compute the wave energy dissipation, from which the wave height (Hs) can be derived. Delft3D-FLOW, besides solving the two and three dimensional shallow water equations, also includes routines to calculate the sediment transport and to update the morphodynamics. The suspended sediment transport is calculated by solving the advection-diffusion equation, the bedload transport with empirical formulations. Hydrodynamics, sediment transport and morphodynamic equations are solved at the computational time step (12 s). The complete set of these models is known as DELFT3D-MOR.

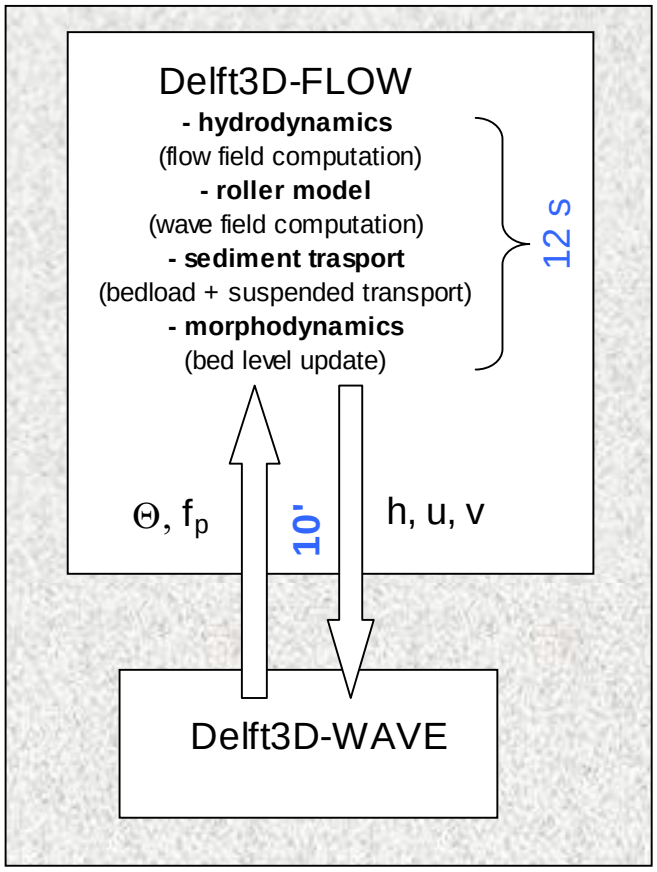

Figure 2.2 Scheme of a morphodynamic simulation in Delft3D-MOR

2.4 Computational grid

A schematized version of the model was used to carry out the different test cases. This schematization corresponds to the reference simulation (Alternative case 0) described in Walstra et al. (2004) and Walstra et al. (2008).

The flow grid was built based on a longshore uniform bathymetry, with a size of 1500 m and 5400 m, respectively in the cross-shore and longshore direction. The grid size ranges between 37 m and 20 m in the cross-shore direction, and it is equal to 40 m in the longshore direction (Figure 2.3). The wave grid size is coarser with a cross-shore and alongshore resolution of 50 m.

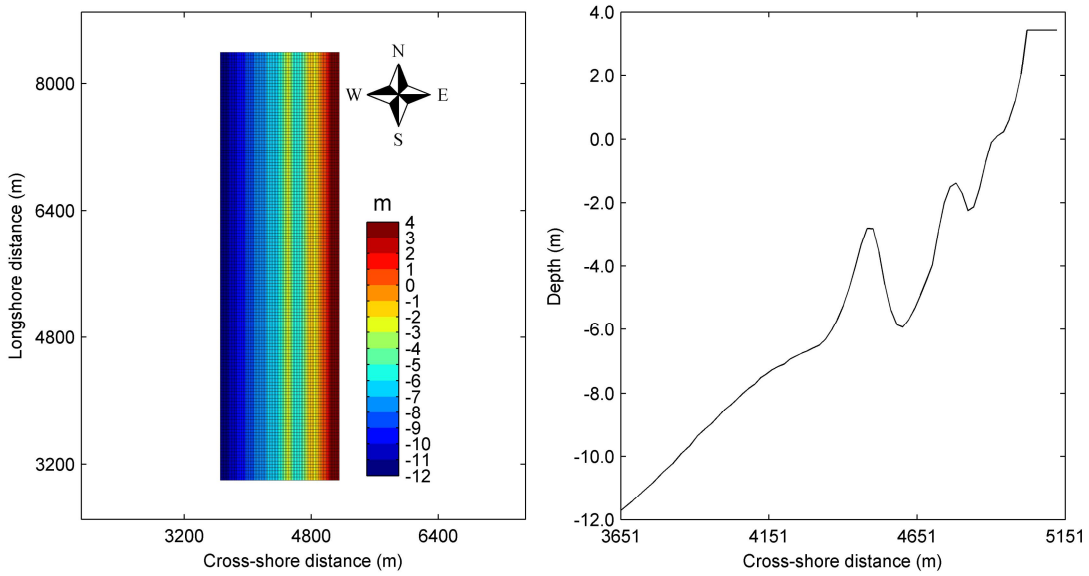

Figure 2.3 *Initial bathymetry and grid of the schematized flow model (left panel), and cross-shore profile (right panel).*

2.5 Boundary conditions

The computational domain is limited by 4 boundaries: three open boundaries (North, West, and South) where the tidal motion is imposed, and one closed boundary (East).

2.5.1 Tidal motion

At the Northern and Southern boundary, the tidal motion was ensured by a longshore gradient in the water level (Neumann boundary) (Roelvink and Walstra, 2004). Due to the limited extension of the model in the cross shore direction, a uniform value of the gradient was assumed along the northern and southern boundary. The sea boundary was forced by a harmonic water level representing a progressive wave in northern direction.

One representative tide was selected and imposed at the Northern and Southern boundary. This representative tide can be described as a superimposition of 6 tidal components (Table 2.1). The selection of the representative tide was done according to the procedure described by Roelvink (1999).

Table 2.1 *Harmonic components at the three open boundaries.*

Frequency	Southern Boundary (Neumann)		Northern Boundary (Neumann)		Sea boundary (harmonic) South		Sea boundary (harmonic) North	
(°/h)	Amplitude (-)	Phase (°)	Amplitude (-)	Phase (°)	Amplitude (m)	Phase (°)	Amplitude (m)	Phase (°)
28.8	1.0552 * 10-5	239.43	1.0583 10-5	239.43	0.70422	149.43	0.70528	153.93
57.6	2.1222 * 10-6	-50.949	1.9849 *10-6	-48.553	0.26068	-140.95	0.25205	-138.55
86.4	2.8119 * 10-7	60.45	4.1933 * 10-7	62.528	0.046531	-29.55	0.056544	-27.472
115.2	1.0348 *10-6	82.212	9.872 *10-7	86.489	0.071632	-7.7882	0.069957	-3.5114
144.0	7.8292 * 10-8	222.21	3.4258 * 10-7	229	0.0069133	132.21	0.12772	139
172.8	4.8295 10-7	219.9	5.4651 10-7	228.69	0.017132	129.9	0.01822	138.69

In order to reduce the computational time, a “morphological acceleration factor” (MorFac) was used (see last column in Table 2.2). This technique is similar to the “lengthening of the tide” method proposed by Latteux (1995). It is well known that the time scale of hydrodynamic changes is much shorter than the one corresponding to the morphodynamic changes. Therefore, changes in bed level after one hydrodynamic time step can be multiplied by a constant “morphological acceleration factor”, in order to speed up the morphodynamic computation.

2.5.2 Wave forcing

In order to minimize the computational time a wave schematization was adopted. This schematization, known as “morphological wave climate”, is described in Van Duin (2002). The wave time series is subdivided into a number of classes with different wave height and direction, each one of them characterized by a probability of occurence. A representative number of waves is then selected in order to get the same gross transport northward and southward, as if all the occurred wave conditions were considered. The morphological wave conditions are schematized in Table 2.2. Influence of wave order schematization on morphodynamic simulations is assessed in Section 4.2.

In the last column, the morphological acceleration factors for the different wave conditions are given. The four wave conditions accompanied by the relative morphological acceleration factors are representative of the net transport occurring in one year period.

Table 2.2 Morphological wave conditions.

Condition	Hs (m)	Tp (s)	Direction (° N)	MorFac
1	2.75	8.3	217	11.142
2	1.25	6.3	217	127.84
3	2.75	9.5	317	8.83
4	1.25	6.3	317	91.04

2.6 Parameter settings

A list including the main parameter settings for the three different modules is given in Table 2.3. For a complete overview of the input files (master definition flow file, master definition wave file, morphology file, and sediment file) refer to Appendix A.

The Delft3D-FLOW model solves the Navier Stokes equations for an incompressible fluid, under the shallow water and the Boussinesq assumptions. The vertical space was discretized in 12 σ-layers with a thickness of 2.0%; 3.2%; 5.0%; 7.9%; 12.4%; 19.6%; 19.6%; 12.4%; 7.9%; 5.0%; 3.2%; 1.8%, of the total water depth, starting from the surface towards the bottom. The time step for the hydrodynamic computation was chosen equal to 12 s. Bottom friction due to currents was calculated according to a Chezy formulation and assuming a constant bottom roughness coefficient equal to 65 $m^{1/2}/s$. The superimposed effect of currents and waves was taken into account by means of the interaction model of Fredsøe (1984). Turbulence effects were computed by means of the *K-epsilon* model. Horizontal background eddy viscosity and diffusivity were set equal to 1 m^2/s. The choice of a value of 1 m^2/s for the background horizontal eddy diffusivity differs to the one used in the work of Walstra et al. (2008), and equal to 0.1 m^2/s. This value has a relevant effect on the hydrodynamics and, as a consequence, also on the morphodynamics of the study area. A value of 10^{-6} was used for the vertical background viscosity and diffusivity.

Wave heights were computed using the roller model (Reniers et al. 2004), included in the Delft3D-FLOW module. The roller model consists of one balance equation for the short wave energy propagation, and another one for the roller energy propagation and wave energy dissipation. Wave energy dissipation due to wave breaking is regarded as the only dissipative mechanism inside the balance equation for the short wave energy. Wave energy dissipation acts as a source term in the balance for the roller energy propagation. Dissipation due to wave breaking was computed according to the formulation of Roelvink (1993), which is an extension of the Battjes and Janssen model (1978). The wave breaking parameter γ was calculated according to Ruessink et al. (2003). The slope β of the wave front on which roller force acts was assumed equal to 0.05. The breaker delay parameterization of Roelvink et al. (1995) was activated in the roller model. Input parameters for the roller model consist of mean wave direction and peak frequency inside the domain, calculated by the Delft-WAVE module. Moreover, the wave energy at the boundary and a value equal to zero have to be prescribed at the open boundary.

The wave computation was carried out by means of a stationary run of the Delft-WAVE module. The model is based on the discrete spectral action balance equation. Wind input was neglected due to the limited spatial extension of the study area. Wave dissipation due to bottom friction was computed according to the JONSWAP model (Hasselmann, 1973), with the default value for the bottom friction coefficient and equal to 0.038 $m^2 s^{-3}$. Depth induced breaking was taken into account by means of the Battjes and Janssen model (1978), where the α and γ parameters were respectively set equal to 1 and 0.73. Whitecapping and non linear wave-wave interactions were neglected.

The coupling time between the Delft3D-FLOW and the Delft-WAVE model was set equal to 10'.

The sediment transport and morphodynamic computation was carried out by means of the Delft3D-SED module. The update expression of the TRANSPOR2004 formula (Van Rijn, 2007 a,b) was used to calculate the bedload and suspended sediment transport. Bed shear stress calculation was based on the Van Rijn (2007 a) roughness predictor. Sediment was assumed to be sandy with a D_{10}, D_{50} and D_{90} respectively equal to 150 μm, 200 μm and 300 μm, and a sediment density equal to 2650 kg/m^3. The dry bed density was set equal to 1600 kg/m^3. Suspended sediment diameter at the beginning of the computation has a representative diameter equal to the D_{50}. A minimum water depth equal to 0.25 m was assumed for sediment transport calculation. The transverse and longitudinal bed slope were set equal to 20. This value is higher than the value proposed by Walstra et al. (2004, 2008) and might result in an excessive flattening of the outer bar.

Parameter	Description	Value
Delft3D-FLOW		
Thick	Vertical distribution of numerical grid (%) (σ-layers, from surface to bottom)	2.0; 3.2; 5.0; 7.9;12.4; 19.6; 19.6;12.4; 7.9; 5.0; 3.2; 1.8
Dt	Time step	12 (s)
Dryflc	Minimum depth for drying and flooding	0.2 (m)
Tkemod	Type of turbulence closure model	K-epsilon
Vicouv	Horizontal eddy viscosity (background value, is determined by local production of turbulence due to breaking waves)	1 (m^2/s)
Dicouv	Horizontal eddy diffusivity	1 (m^2/s)
Vicoww	Vertical eddy viscosity (background value, is determined by local production of turbulence due to breaking waves)	1.0E-6 (m^2/s)
Dicoww	Vertical eddy diffusivity (background value, is determined by local production of turbulence due to breaking waves)	1.0E-6 (m^2/s)
Rhow	Water density	1023 (kg/m^3)
Rhoa	Air density	1.0 (kg/m^3)
Roumet	Type of bottom friction formulation	Chezy
Ccofu, Ccofv	Bottom roughness coefficient in the –u and –v direction	65 ($m^{1/2}$/s)
Rouwav	Bottom stress formulation due to wave-current action	Fredsøe (1984)
F-lam	Breaker delay parameter (Roelvink et al. (1995)) in roller model	- 2
GamDis	γ-expression (wave height to water depth ratio) in roller model	Ruessink et al. (2003)
Betaro	Slope of wave front on which roller force acts in roller model	0.05
Delft3D-WAVE		
-	Model for bottom friction	Jonswap
Γ	Bottom friction coefficient	0.038 (m^2 s^{-3})
-	Model for depth induced breaking	Battjes and Janssen (1978)
α	Calibration coefficient in Battjes and Janssen (1978) formulation	1

γ	Wave height to water depth ratio in Battjes and Janssen (1978) formulation	0.73
Delft3D-SED		
Trafrm	Sediment transport formula	Van Rijn (2007)
-	Roughness predictor	Van Rijn (2007)
SedD10	Sediment diameter for which 10 % is finer	150 (μm)
SedDia	Median grain size	200 (μm)
SedD90	Sediment diameter for which 90 % is finer	300 (μm)
RhoSol	Sediment density	2650 kg/m^3
CDryB	Dry bed density	1600 (kg/m^3)
FacDSS	Factor for defining suspended sediment diameter FacDss * SedDia	1.0
SedThr	Minimum depth for sediment calculation	0.25 (m)
Alfabn	Transverse bed slope	20
Alfabs	Longitudinal bed slope	20

Table 2.3 List of the main numerical parameters used for the numerical simulations.

2.7 Changes to the standard Delft3D code

A number of changes and improvements have been made in this project to the sediment transport and morphology routines in Delft3D, as well as in the roller model routines. The changes have been made in delftflow version 3.60.00.6356.

In 3D simulations, Delft3D generates oblique sand bars along the coast line. These do not appear to be realistic and can lead to numerical instabilities. The oblique bars, which typically develop when waves attack the coast at angles smaller than 30 degrees with respect to the shore normal, eventually grow so large that they start to influence even the behaviour of offshore bars. This has prevented us so far from running 3D simulations for periods longer than a few months. Most of the changes described in this section are implemented in order to prevent or reduce the formation of oblique bars. It appears that there are two main causes for the development of oblique bars: underestimation of alongshore wave driven currents and the numerical scheme that is applied in the advection/diffusion solver for suspended sediment transport. The first issue has been dealt with by altering the bed shear stress formulations (Section 2.7.1). The second issue has been solved by changing the advection/diffusion scheme (Section 2.7.2).

Some fixes have also been made in the roller model, which produced unrealistic results near hard structures such as thin dams and dry points (Section 2.7.3).

In addition to improvements in the sediment transport and roller code, two other new features have been added to the standard code this year:

Quasi-3D approach (Section 2.7.4)
Beach and dune module (Section 2.7.5)

These additions have been partially developed and improved within the Kustlijnzorg project, although they have not actually been applied in the project itself.

2.7.1 Bed shear stress in surf zone

The formation of oblique bars in 3D simulations is partially caused by an underestimation of alongshore wave driven currents, which (to some extent) smooth out alongshore bathymetric variations. In Treffers (2009), a new approach of computing the bed shear stress is presented which yields a better representation of the alongshore velocities. The approach is briefly described here.

The longshore currents in the surf zone in the 3D approach are underestimated (up to a factor two for small angles of incident waves) independent on the chosen wave climate. Reducing the thickness of the computational layer, results in a further underestimation of the wave-driven longshore currents in the surf zone. This is due to the method used for computing the bed shear stress in the 3D approach in the presence of waves. Wave-breaking induces enhancement of vertical mixing, resulting in a more vertically uniform distribution of the longshore current. Therefore, the assumption of a logarithmic vertical distribution is no longer valid. In the standard version, bed shear stress is computed by means of the velocity at the height of the first layer above the bottom, assuming a logarithmic velocity profile. In case of wave breaking, when the profile differ from the logarithmic one, this results in an overestimation of the flow-induced bed shear stress and therefore the flow velocity becomes lower if the thickness of the computational layer just above the bed decreases. The layer dependency can be overcome by calculating the shear stress by using the velocity in a fixed point in the vertical, which is independent on the thickness of the bottom computational layer. The top of the wave boundary layer was chosen as an appropriate fixed point above the bed. A description of the changes applied to Delft3D code for improving the bottom friction calculation is given in Table 2.4.

The new method of computing the bed shear stress is validated using the laboratory experiments performed by Reniers and Battjes and also validated using field measurements at Sandy Duck, North Carolina, USA. Both the 2DH and 3D approach corresponds reasonable well with measurements. The longshore flow velocity near the shore is generally overestimated. This is also the case for the wave height computed using the roller model, which shows a systematically overestimation compared with measurements. The advantage of the 3D approach is that it computes a vertical distribution of the currents. This is also validated using the SandyDuck97 measurements and showed that the computed vertical distribution corresponds reasonably well with the computed distributions.

Table 2.4 Changes in bed shear stress routines

Routine	Description
taubot.f90	Thickness of wave boundary layer is computed. Imaginary 2Dh current velocity is now determined using the velocity in the first layer above this thickness. Keyword added to mdf file is Wbndly (default = 0.0). Wbndly = 0.0 (default) -> using velocity in bottom layer (original implementation) Wbndly = -1 -> using velocity above wave boundary layer (new

	implementation Wbndly > 0.0 -> using velocity in layer above Wbndly
dwnvel.f90	Similar changes applied as in taubot.90.
erosed.f90	Call to dwnvel.f90 changed to include wave parameters hrms, tp and rlabda (used to compute wave boundary layer).
rdnum.f90	Changed to read in keyword wbndly

2.7.2 Changes in sediment transport routines

The advection / diffusion solver of Delft3D applies a third order upwind scheme to compute suspended sediment transport. This approach can lead to a reversal of the transport direction in case of large horizontal sediment concentration gradients. This appears to be one of the driving forces behind the generation of unrealistic oblique sand bars along the coast. Due to the large horizontal gradients in suspended sediment concentrations over these bars (high at the top of the bar, low in the downwind trough) the sediment transport at the downwind side can actually change direction by 180 degrees. This leads to more deposition at the top of the bar, and even higher horizontal concentration gradients. There is, in other words, a positive feedback between the growth of the oblique bars and the reversal of the transport direction.

In order to solve this problem, a simpler 1st order upwind scheme has been applied. This strongly reduces the formation of oblique bars, without significantly altering the morphodynamic behaviour in other areas.

Some other changes have also been been made, mostly dealing with fixing errors in the sediment mass balance. A description of the changes applied to the Delft3D code to the sediment transport routines is given in Table 2.5.

Table 2.5 Changes in sediment transport routines

Routine	Description
difu.f90	Applying first order upwind scheme for sediment transport when using keyword FirstOrderUpwind = true in mor file
red_soursin.f90	Maximum erosion flux limited to available sediment at the bed (in order to reduce negative sediment thickness at bed).
erosed.f90	Computes bed level gradient (slope) in cell centre. Used in bedbc2004.f90. Used to be slope with on u and v point same m,n index, which lead to grid orientation dependencies.
calsinkse.f90	Multiplies sinks (computed in difu) with sediment concentrations in kmxsed layer before forrester filters are applied. This is needed to make the sink terms consistent with the terms in BOTT3D. Otherwise mass balance errors may occur.
tritra.f90	Calls calsinkse.f90
bott3d.f90	Now using sediment sink term computed in calsinkse.f90.
bott3d.f90	In stage 2 (second half time step) suspended and bed load transports (use only for output) are averaged with transports from stage 1. This prevents inconsistencies in output between transports and bed level changes.

caltmx.f90	Only for cohesive sediment: bed shear stress in cell centres is computed in similar way as in downvel.f90. Prevents the development of checkerboard patterns in bed level.

2.7.3 Changes in roller model routines

The combination of the roller model and hard structures (dry points and thin dams) or dry cells in the standard version of Delft3D leads to errors. These are caused by the fact that hard structures and dry cells do not dissipate (or reflect) incoming wave energy. As a result, a strong build up of wave energy occurs where wave energy hits these points. This typically leads to large orbital velocities and strong erosion near structures. In deeper water, the build up continues until the wave start breaking. The resulting wave forces can lead to strong erroneous currents near structures. In shallow water, in wet grid cells next to the water line, the wave height can also be overestimated.

The poblem has been fixed by altering the numerical scheme of short wave and roller energy propagation near structures and dry points. It has been implemented in such a way that wave and roller energy does leave grid cells adjacent to structures and dry cells, but no energy can enter the grid cell down wind of the hard structure. Structures and dry cells thereby effectively dissipate incoming wave energy. The routines that have been altered are described in Table 2.6.

A number of other minor changes have been made to the roller model code. These also mostly deal with the numerical scheme and should fix some problems with overestimations of wave heights on cell interfaces (kfu and kfv points).

Table 2.6 Changes in roller model routines

Routine	Description
difuwe.f90	Changed the numerical scheme at closed cell interfaces (kfu=0 and kfv=0) in order to dissipate incoming energy through these interfaces.
qkwcg.f90	Short wave and roller energy velocities no longer set to 0.0 in closed cell interfaces (now using upwind velocities instead). This is needed to make the changes in difuwe.f90 work.
massfl.f90	Applying central scheme for wave mass flux. Wave mass flux at cell interface used to be the same as massflux of cell with the same m,n indices (this lead to grid orientation dependencies).
orbvel.f90	Now computing wave length rlabda every time step. Made more consistent with other routines.

2.7.4 Quasi-3D approach

Due to the large calibration effort and especially the large computational time, fully three-dimensional (3D) simulations are often not very practical in engineering applications. Therefore, many of these morphological studies are carried out in the depth-averaged (2DH) mode. Several projects have shown that especially in depth-averaged mode the present possibilities to adjust the cross-shore transport in the nearshore area, and the associated cross-shore profile developments, are inadequate.

Based on these drawbacks it was decided to implement, validate and evaluate a new approach in Delft3D which represents the 3D results in the nearshore zone, but with less computational time. This work has been carried out in 2008 and is described in detail in Henrotte (2008).

When considering the depth-averaged current field to be representative of the entire flow pattern, one makes the implicit assumption of vertical similarity of the velocity profile, i.e. the velocity profile in every point in the horizontal has the same shape (e.g. logarithmic). In reality, however, the velocity field is more complex than this. This particularly holds in nearshore areas where breaking waves cause (secondary) return flow currents. To reproduce these secondary currents a quasi-three dimensional (Q3D) model based on the concepts of Reniers et al. (2004) was implemented into the Delft3D model. This model computes the vertical velocity distribution at every grid point accounting for tidal forcing, wave breaking, wind and dissipation due to bottom friction. Validation of the Q3D approach was carried out on four validation cases: three flume experiments (LIP, Boers and Reniers) and one field case (Egmond).

The initial implementation was carried out in a relatively old research version of Delft3D. Within the Zandmotor project, the quasi-3D approach has been built into the most recent Delft3D version (delftflow version 3.60.00.6356). In addition, a number of improvements to the Q3D method have been made with respect to the work carried out in 2008. These are described here.

For a detailed description of the quasi-3D approach reference is made to Henrotte (2008). This section of the report only describes the recent improvements.

In the original approach, representative sediment concentrations were computed based on the absolute suspended transport and the absolute depth-averaged eulerian velocities.

crep = Sabs / uabs

These representative concentrations (crep) were used in the advection-diffusion solver, where they are transported with the eulerian velocities. The direction of the sediment transport in the transport solver, which solves the advection diffusion equation, was not necessarily the same as the direction as computed in the sediment transport routine EQTRAN. In theory, it was possible that the eulerian velocities were directed onshore, whereas the sediment transport (due to wave-breaking induced undertow) was actually directed offshore.

In the new approach, suspended sediment transports are computed in both alongshore and crosshore direction (S_x and S_y) in EQTRAN using the GLM velocities, as well as the depth-averaged sediment concentration (c_{avg}) in each grid cell. Reprentative depth-averaged

velocities are computed by dividing the transports in both directions by the depth-averaged concentrations:

$U_{rep,q3d} = S_x / c_{avg}$

$V_{rep,q3d} = S_y / c_{avg}$

In the advection-diffusion equations, the depth-averaged sediment concentrations are now transported using these representative U and V velocities ($U_{rep,q3d}$ and $V_{rep,q3d}$). In this way, not only the transport magnitude that is computed in EQTRAN is correctly computed in the advection-diffusion solver, but also the transport direction.

Table 2.7 Changes for quasi-3D approach

Routine	Description
vsm_u.f90	Computes quasi-3D velocity profiles
eqtran.f90	Calls vsm_u.f90, computes Q3D sediment transport in u and v direction, computes depth-averaged concentration and determines representative u and v velocities for advection – diffusion solver.
erosed.f90	Computes representative u and v velocities in velocity points.
q3dcor.f90	Computes fluxes qxk and qyk for difu.f90 with representative Q3D velocities.
tritra.f90	Calls q3dcor.f90.
rdmor.f90	Reads Q3D parameters from mor file.

2.7.5 Beach and dune module

2.7.5.1 Description

Delft3D is often applied to simulate the short and medium term morphodynamic development of coasts. Several processes that govern the behaviour of the intertidal area, dry beach and dunes are not (or at least not properly) taken into account by Delft3D. It lacks for example reliable formulations for swash and dune erosion caused by storm surges. Dune erosion and growth due to aeolian transport are not modelled at all by Delft3D.

An attempt has been made to model the effect of these processes on the longterm behaviour of the dry beach profile. An analysis of historical data that was undertaken previously (De Vriend and Roelvink, 1998) has shown that the beach width along the Dutch coast (distance between low water line and dune foot) tends towards an equilibrium of approximately 125 m. If the actual beach is wider than this equilibrium, the dunes will grow and the dune foot line (NAP +3m) shifts towards the sea. If the width is smaller, the dune will erode and the dune foot line will migrate landwards. The speed at which the migration occurs is proportional to the difference between the actual beach width and the equilibrium width:

$$v = \alpha(L - L_{eq})$$

The factor α depends on whether the beach width is wider or smaller than the equilibrium. The erosion of the dune (which takes place when the beach width is smaller than the equilibrium) occurs at a much faster rate than the accretion that happens when it is wider.

Erosion: α = 0.080 / year

Accretion: α = 0.024 / year

2.7.5.2 Implementation

A dune module has been developed for Delft3D that simulates this horizontal migration of the dune foot. It assumes that the entire dry profile will shift at the speed of the dune foot migration while retaining its shape. At each time step, at the end of the 'regular' bed updating routine *bott3d.f90*, the beach width is determined for each cross shore grid line and the dune migration speed for each grid line is computed. After this, the beach profile in each grid line is updated.

The bed level change of each grid cell in the dry profile is computed with:

$$\frac{\partial z}{\partial t} = v\frac{\partial z}{\partial x},$$

where $\partial z / \partial x$ is slope of the beach and v is the migration speed.

The total volume gain or loss in the dry profile is either taken from or redistributed within the first ten wet grid cells that are the most located near the shoreline. This is necessary to ensure conservation of mass.

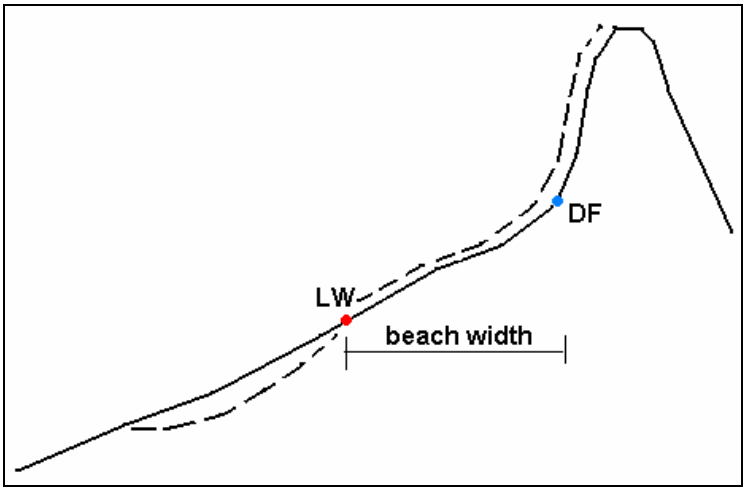

Figure 2.4 Definition of beach width

2.7.5.3 *Model results*

The dune module was first successfully tested on the Egmond bathymetry of November 2004 with a simple Matlab script. Sediment transport processes in the nearshore zone were not taken into account in this test. The idea however was that even without this sand transport, the beach width should tend to an equilibrium. The following figures show the initial bathymetry and the bathymetry after 50 years. The blue line in the left panel indicates the position of the low water line whereas the black line shows the position of the dune foot. On the right panel, the upper figure shows in black the beach width on a longitudinal profile. The red dashed line represents the equilibrium beach width. The lower figure shows the migration velocity of the dune foot on a longitudinal profile. Positive growth rate are symptom of a landward retreat of the dune foot.

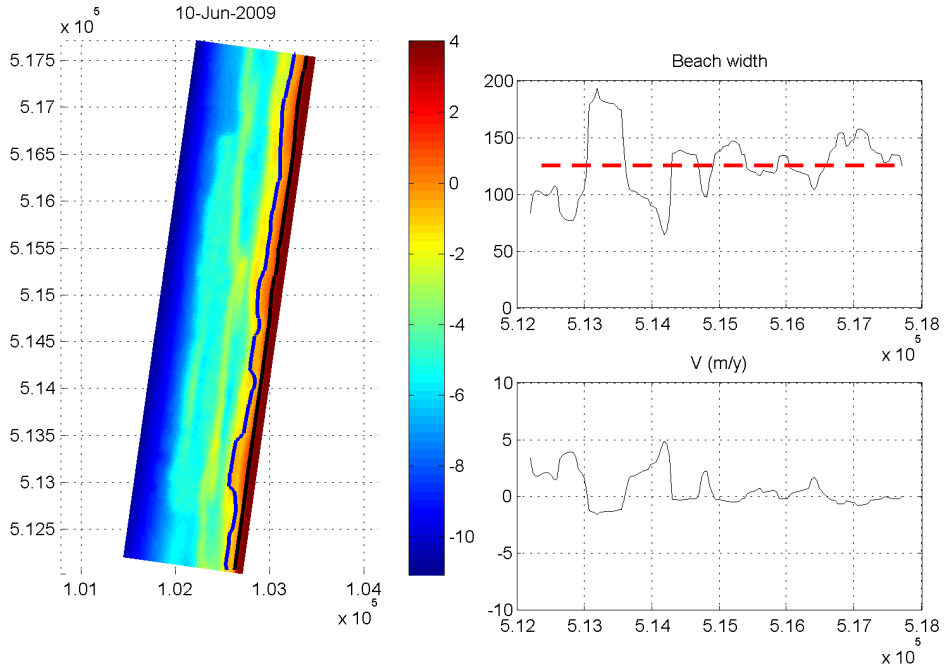

Figure 2.5 Initial bathymetry Egmond

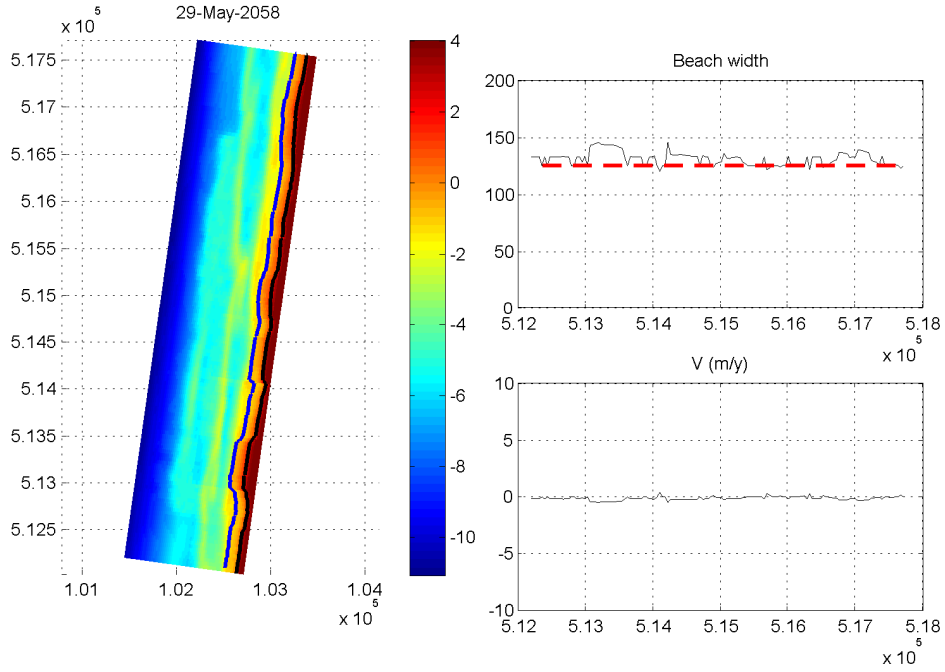

Figure 2.6 *Bathymetry Egmond after 50 years*

The next step was to test the module in Delft3D. The following figures show the results of a test case with a simple model. It is a 'classic' schematisation of a straight coast with a groyne and waves coming in at an angle of 45 degrees. The model shows accretion to the west of the groyne and erosion to the east (Figure 2.7). The evolution of profiles 1 and 2 can be seen in Figure 2.8. In profile 1, accretion takes place on the dry beach, whereas in profile 2 the dry beach is eroding. This is solely the effect of the dune module. The regular Delft3D bed updating routines do not compute any bathymetric changes on the dry beach.

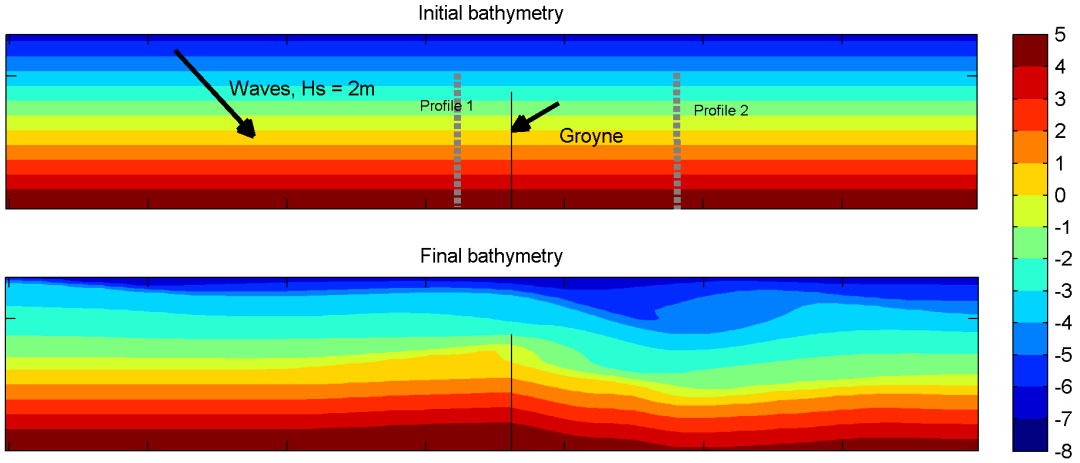

Figure 2.7 *Bathymetric evolution*

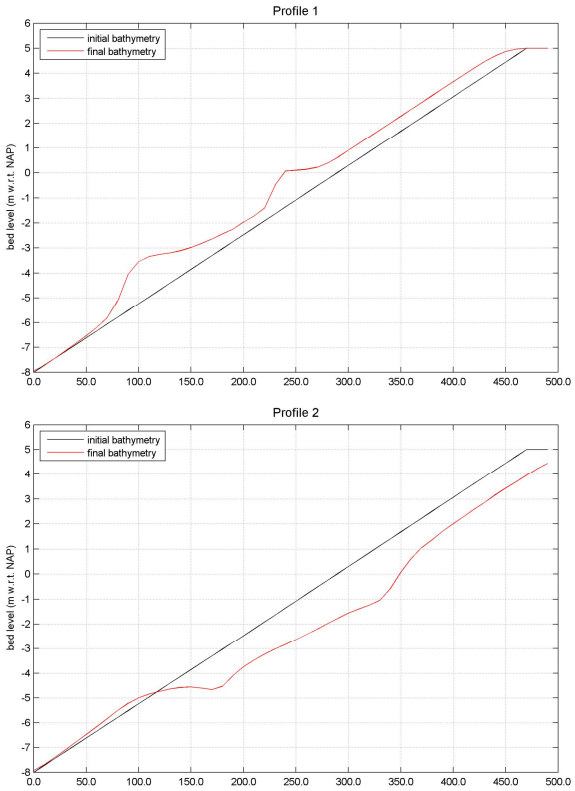

Figure 2.8 Profile evolution

The dune module in Delft3D appears to be a computationally efficient way to compute the migration of the dune line. However, it needs to be properly validated against field data. Further tests are therefore ongoing. At present we are doing a historical hindcast around the port of IJmuiden, and some longterm simulations of the Zuid Holland coast have also been carried out. The changes in the beach-dune module have been summarized in Table 2.8.

Table 2.8 Changes for beach-dune module

Routine	Description
beachwidth.f90	Computes beach width at each time step and redistributes sand between surf zone and dry beach.
bott3d.f90	Calls beachwidth.f90
rdmor.f90	Reads beach dune module input parameters

2.7.6 Comparison between standard version and adjusted version

A simple model of a straight coast is used to test the effects of the new Delft3D version. A constant beach slope of 1:50 is applied. The model is approxmately 2.5 km long and 1 km wide. Tide effects (water levels and currents) are not included in the simulations. The wave boundary condition is constant in time (H_{sig} = 1.5 m, T_p = 6 s, direction 20º to shore normal). The simulations are run over a 10 day (morphological) period (MORFAC = 50). The bottom panels of Figure 2.9 shows the alongshore current magnitude for the standard and updated version. The new implementation of the bed shear stress computation leads to an increase in horizontal velocities of approximately 30 %. The top panels show the bed level after 10 days

for the two versions. A much smoother, more realistic looking result is obtained with the new version, although oblique sand bars are still developing.

A further analysis of the results obtained with this new Delft3D version of the code is given in Chapter 3 and 4, respectively for different angles of wave attack and for a nourishment scenario.

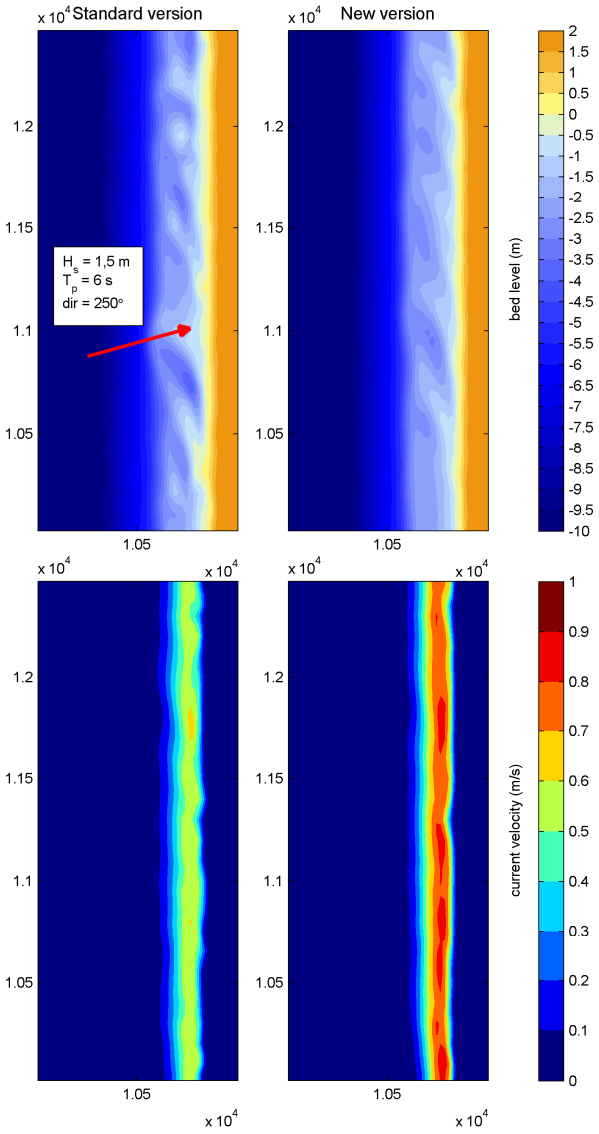

Figure 2.9 *Straight coast, comparison between standard and new version. Upper panels: bed level after 10 days, lower panels: initial current magnitude*

The morphodynamic simulations that were run within the Kustlijnzorg (2008) study for Egmond were repeated with the standard and new Delft3D version. The top panel of Figure 2.10 shows the results of the standard version, whereas the bottom panel the results of the new version. In general, both simulations show good agreement with the observed bed level changes. Especially the alongshore movement of sand bars appears to be modelled quite

well in both cases. Sand bars however (especially the inner bar) seem to be flattened out too much by both the standard in the new version. The most striking difference between the two simulations is the fact that the oblique sand bars that appear in the standard version develops at much lesser extents in the new version.

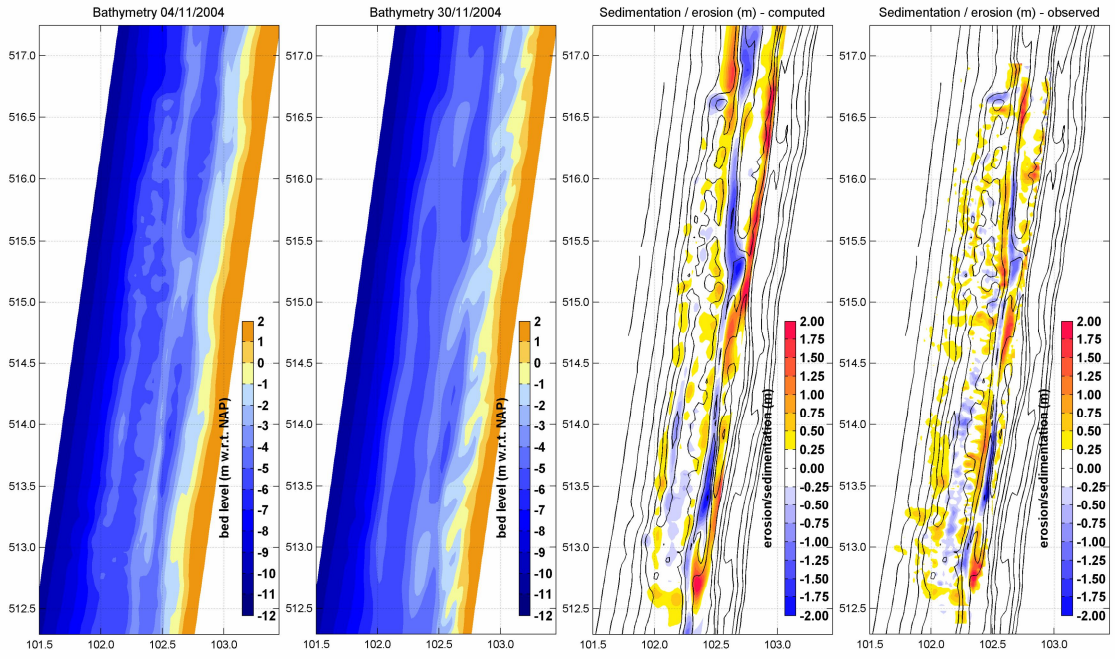

Figure 2.10 *Computed bathymetry Egmond (November 2004) and computed vs. observed sedimentation/erosion (standard version)*

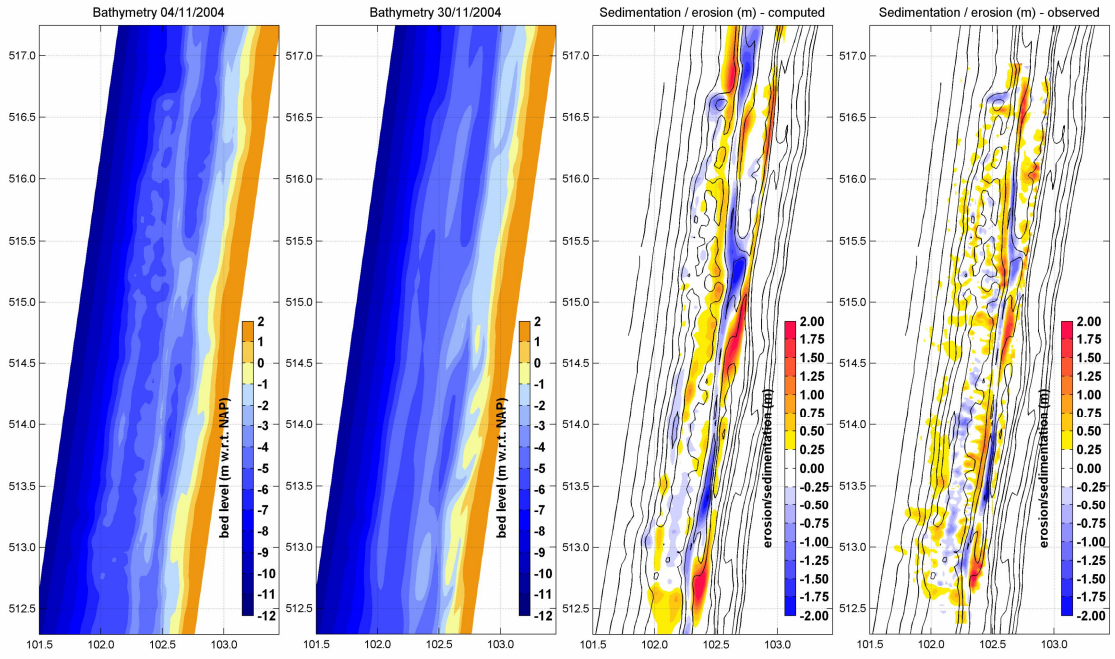

Figure 2.11 *Computed bathymetry Egmond (November 2004) and computed vs. observed sedimentation/erosion (updated version)*

2.7.7 Recommendations / future developments

The present version of Delft3D typically predicts too much erosion near the water line. One of the culprits may be the way in which the correction of roller mass flux at the water surface on sediment transport is implemented. Right now, the correction for mass flux in the roller model is applied uniformly over the water depth. This may lead to an overestimation of near-bed offshore-directed velocities, and, as a result, an overprediction of offshore-directed sediment transport in the surf zone. By applying a more realistic distribution of the correction over the water depth, this problem may be overcome.

Offshore sand bars appear to be smoothed out too much in morphodynamic simulations. Preliminary tests with a profile model have shown that this may be partially related to numerical scheme of the bed load transport which uses an upwind approach. Applying a central scheme (set keyword in mor file UpwindBedload = false) shows much less smoothing of sand bars, and may be (part of) the solution to maintain the correct shape of sand bars. A further investigation are needed to test this.

3 Influence of wave attack angle on bedform formation.

3.1 Introduction

Earlier applications of the Delft-3D model for long term morphodynamic simulations have shown one significant limitation: along the beach line, regular bedforms were forming, and growing out of control especially during low wave activity periods (Walstra et al., 2008). Due to the uncontrolled growing of the bed forms, morphodynamics simulations have been so far limited to a period no longer than one month.

On the other hand, previous studies have shown that the Dutch coastline might be potentially unstable under specific wave conditions. This would lead to the growing of irregularities such as transverse bars and rips (Falqués, 2008). The presence of rhythmic features at the central Netherlands coast is also proved by observations (Short, 1992).

The challenge consists in identifying at which extent these features are related to natural instability of the system and, on the other hand, what could be simply related to model inaccuracies. In the second case, the model should be corrected and improved, to allow the simulation of long term processes at the time scale of years. Purpose of this Chapter is to discuss and test modifications to the standard Delft-3D code, which would possibly lead to an improvement of the simulation results. Moreover, natural instabilities of the system are discussed in relation with their driving forces: waves, rip currents, and longshore currents.

Paragraph 3.2 includes a literature review concerning the formation of alongshore quasi-rhythmic features. In Paragraph 3.3 the model schematization and boundary conditions are described. On this geometry several test cases were carried out, at first, with the standard version of the code (Paragraph 3.4). Different wave angles were assumed, in order to show the relative impact of wave activity and long shore currents on the growing of these bed forms.

In Paragraph 3.5 the same test cases as in Paragraph 3.4 were repeated, but adopting the modified version of the Delft-3D code, as described in Paragraph 2.7.

3.2 Longshore bottom features review

The modelling of coastal morphodynamics is one of the most complex disciplines in ocean engineering due to the presence of multi-scale nonlinear processes, involving currents, waves, and sediment transport all coupled to the changing topography. Reality often shows that the solution of this non linear system in terms of shore evolution reflects into complex patterns, characterized by a certain alongshore regularity. These quasi-rhythmic bottom features might evolve into rip channels, mega cusps, beach cusps, etc. according to their length scales. One of the first attempt to explain the presence of rip currents was proposed by Munk (1949). He suggested that the presence of rip currents provides an equilibrium mechanism against the piling up of water transported onshore by wave action. This theory has been recently extended in order to estimate the current velocity inside the rip channels.

More generally, two groups of theories have been proposed to explain the growing of these bedforms (Falqués et al., 1996; Castelle et al., 2006). The first one relates the presence of bed-flow instabilities to standing edge waves. However, bed-flow instabilities have been observed even when no change to the external forcing occurs (Reniers et al. 2004). The second one relies on self-organization mechanisms and on the strong feedback between hydrodynamics and morphodynamic changes, which allows the development of instabilities.

Falqués et al. (1996) showed that the combined system of a longshore current flowing on an erodible beach can be unstable due to the positive feedback between flow and topographical disturbances. His conclusions were based on a numerical model solving the depth average momentum equation and mass conservation, coupled to a sediment transport and sediment conservation equation at the bottom. The instability was generated as a result of the vertical vorticity generated by the topographically induced differences in bottom friction.

A more extended work was carried out by Falqués et al. (2008). Results from five different models were compared including linear and non linear stability models. The influence of wave activity was also taken into consideration. As a result of this investigation, it was shown that a shore parallel bar may develop rip channels and become crescentic just by self-organization of the coupling between flow and morphology. Larger wave breaking would occur over the shoals than at the channels. This would result into a circulation cell with onshore flow over the shoals and offshore flow over the channel.

The effects of wave directional spreading into the morphodynamic response were examined in Reniers et al. (2004). Their numerical model consisted of a shallow water flow model, coupled to a sediment transport and morphological model, and forced by wave groups obtained from a directional spectrum with a mean wave angle normal to the shore. Their work showed how rip spacing relates to the directional spreading of the short waves. Another important conclusion was that the computed infragravity contribution was not required to generate the quasi-periodic response of the beach.

A good literature review concerning rip currents is given by MacMahan et al. (2006).

3.3 Model schematization and boundary conditions

Different simulations were carried out adopting the model schematization described in Chapter 2. A Neumann boundary was prescribed at the Northern and Southern boundary. The sea boundary was forced by a harmonic water level.

The wave forcing was simplified to one only wave condition with Hs equal to 2 m and Tp equal to 8 s. Different angles of wave attack were tested, respectively equal to 270°, 290 ° N, and 310° N, where the angles are defined according to the Nautical convention (e.g. the direction where the waves come from, measured clockwise from geographic north).

The length of each simulation is equal to one tidal cycle (12.5 hours). The morphological acceleration factor was set equal to 10 for all the simulations. Therefore, the morphodynamic evolution corresponds to the one obtained after 10 tidal cycles. All the other numerical parameters correspond to the ones described in Paragraph 2.6.

3.4 Numerical simulations on a schematized bathymetry with standard Delft-3D code

The computed final bathymetry, for wave angles of 270°, 290°, and 310° is shown in Figure 3.1. The Figure shows the appearance of multiple rip channels in the computed bathymetry when the angle of wave attack is equal to 270° and 290°. Given the fact that initially there is no longshore variation in the bathymetry and in the external forcing, this suggest that the development of quasi-periodic features is related to self organizing properties of the morphodynamic system. This leads to a positive feedback between the bed and the hydrodynamic conditions. The initial perturbation necessary to the start of the self organizing process are small errors within the computation (Reniers et al., 2004).

Moreover, the Figure illustrates the high influence of wave direction on the morphodynamic evolution. In case of wave coming with an angle of 270°, the final bathymetry shows the formation of the biggest bedforms. These rhythmic features develop along the shore, reaching the outer bar at the end of the simulation. Figure 3.2 shows the computed bedforms

for different longshore transects: at the outer bar, at the inner bar, and in the swash zone. For wave coming with an angle of 270°, their predicted wavelength is about 180 m. The computed amplitudes are overpredicted with respect what can be expected in reality. Moreover, their spatial extension up to the outer bar is not physical. A key role in controlling the growing of these bedforms is played by the longshore currents, acting as a smoothing mechanism against the formation of rips. In case of waves perpendicular to the coast, the gradient in radiation stress in the longshore direction is equal to zero. It follows that longshore currents due to wave breaking are also nil.

For waves coming from an angle of 290°, the computed bathymetry still shows the presence of a quasi-periodic bathymetry, but of smaller magnitude, especially at the outer bar and inner bar. The wave length of these forms is also larger (about 400 m). This behaviour follows the findings of Falques et al. (2008), who predicted an increase in wave length from 211 m to 411 m when the wave angle changed from perpendicular to an angle of 80° with the shore line. Their shape is clearly asymmetric due to a wave field coming from the North West, generating northerly longshore currents. A similar behaviour was derived from observations and modelling results at the Aquitanian coasts (Castelle et al. 2005). According to the authors, long periods of oblique swell resulted into a dissymmetric crescent shape of the bedforms.

For the final situation (waves coming from an angle of 310°), no bedforms are visible at the end of the simulation, and the bathymetry appear very similar to the initial one. Longshore currents are in this case the dominant process due to the higher wave angle, and play a major role in preventing the formation of rip channels and quasi-period bottom features.

The instantaneous velocities at the bottom layer for the three simulated cases are shown in Figure 3.3. In the first case, ripple currents are clearly visible in the rip channels, forming a series of vortexes along the shore. Figure 3.4 shows a zoom on some of these vortexes. Rip currents are parallel to the bedform crests at the offshore side of the recirculation cells, they veer near the beach and give rise to a return flow inside the rip channels. The positive feedback between the bed and these quasi-periodic hydrodynamic conditions leads to the growing of the undulations in the bathymetry. The growing of these forms seems to reach stabilization at the end of the simulated period.

The same simulations were also run in 2D mode (not shown). A similar quasi-rhythmic pattern was observed at the end of the simulation. This confirms that the rip generating process is, in first place, a two dimensional process.

To conclude, the formation of quasi-rhythmic features is a physical process, which can be observed in nature and proved by numerical calculation. The Delft3D model is able to represent the formation of these features. However, the amplitude and spatial extension of these features are overpredicted, limiting the possibility of running long term computation. Improvement to the standard Delft3D code are necessary, in order to be able to correct represent these bottom features (Section 3.5).

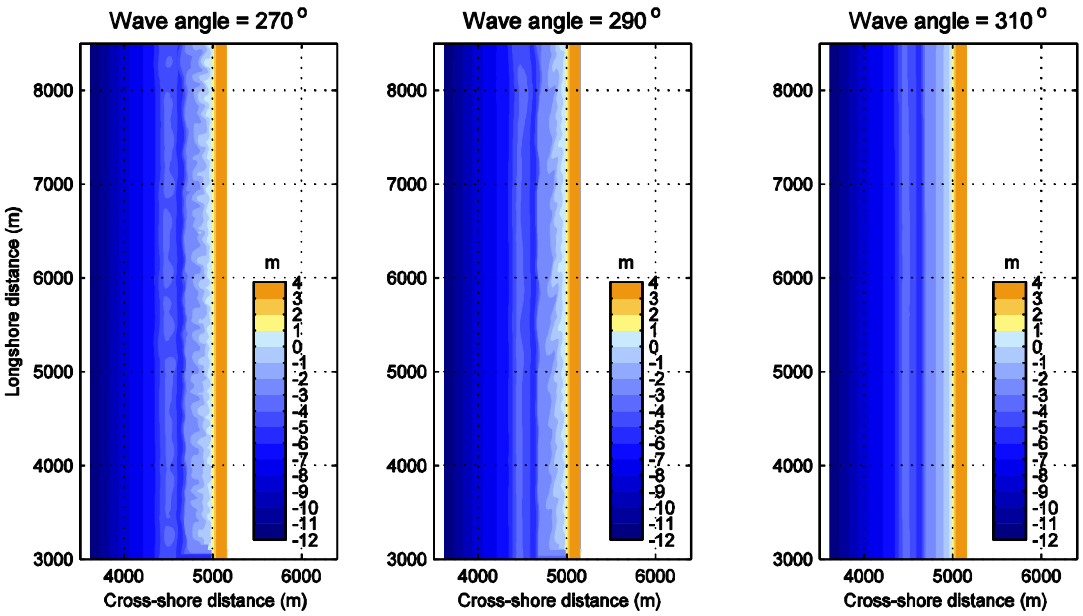

Figure 3.1 *Computed bathymetries after 10 tidal cycles and for different wave conditions. Wave angle = 270° (left panel), wave angle = 290° (middle panel), wave angle = 310 ° (right panel).*

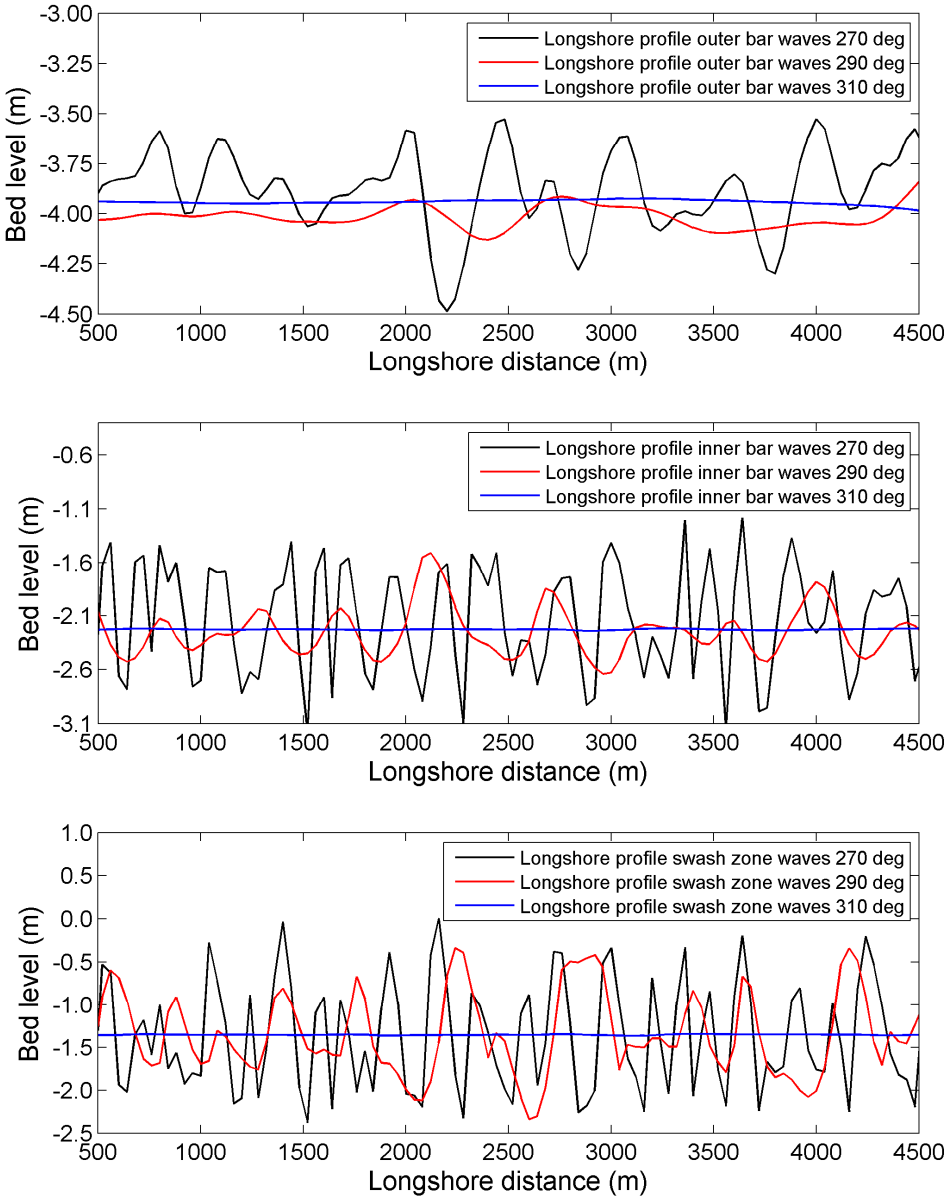

Figure 3.2 *Computed longshore bottom profiles for different wave angles at different cross-shore position: at the outer bar (upper figure), at the inner bar (middle figure) and in the swash zone (lower figure).*

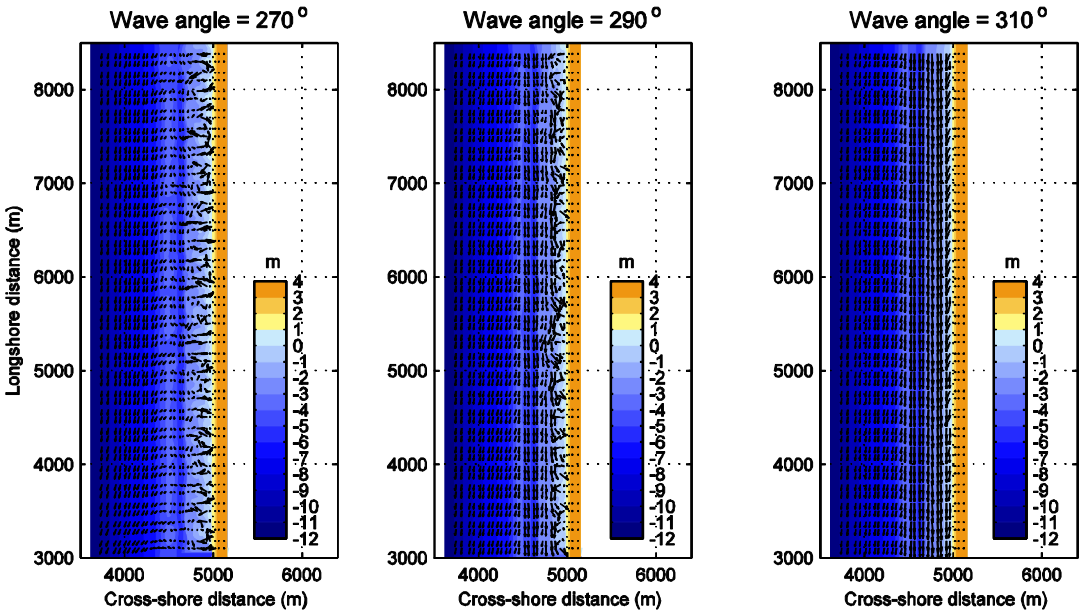

Figure 3.3 *Same as Figure 3.1, but velocity vectors at the bottom layer after 10 tidal cycles are added to the final bathymetry.*

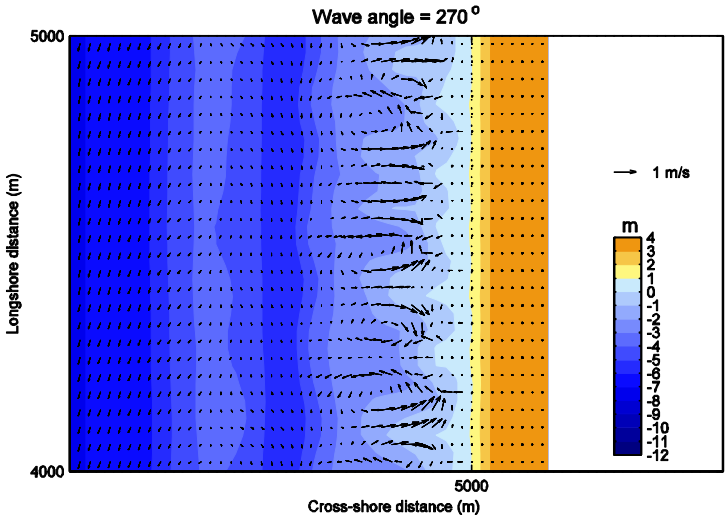

Figure 3.4 *Rip currents and simulated bathymetry in case of waves coming from a 270° angle.*

3.5 Numerical simulations on a simplified bathymetry with modified Delft-3D code

The same simulations carried out in Section 3.4 were repeated including the changes to the standard Delft3D code, as described in Section 2.7. The computed bathymetry for different wave conditions is shown in Figure 3.5. If compared with Figure 3.1, the bathymetry computed with the modified version of the Delft3D code, shows a much more controlled growth of the alongshore bedforms. The difference is especially visible for waves coming from an angle equal to 290°. Also the vortexes and rip currents nearly disappear when the wave angle increases from 270° to 290° (Figure 3.6). Computed alongshore profiles show a much more regular profiles with bedforms of smaller amplitude, especially for a 290 wave angle (Figure 3.7). The outside bar is nearly unaffected by the quasi-rhythmic features. This supports the results obtained in Paragraph 2.7.6. From these results, we can conclude that the modifications applied to the standard Delft3D code can in principle lead to an

improvement of the morphodynamic simulation results. However, further testing with real bathymetry data is necessary before drawing final conclusions.

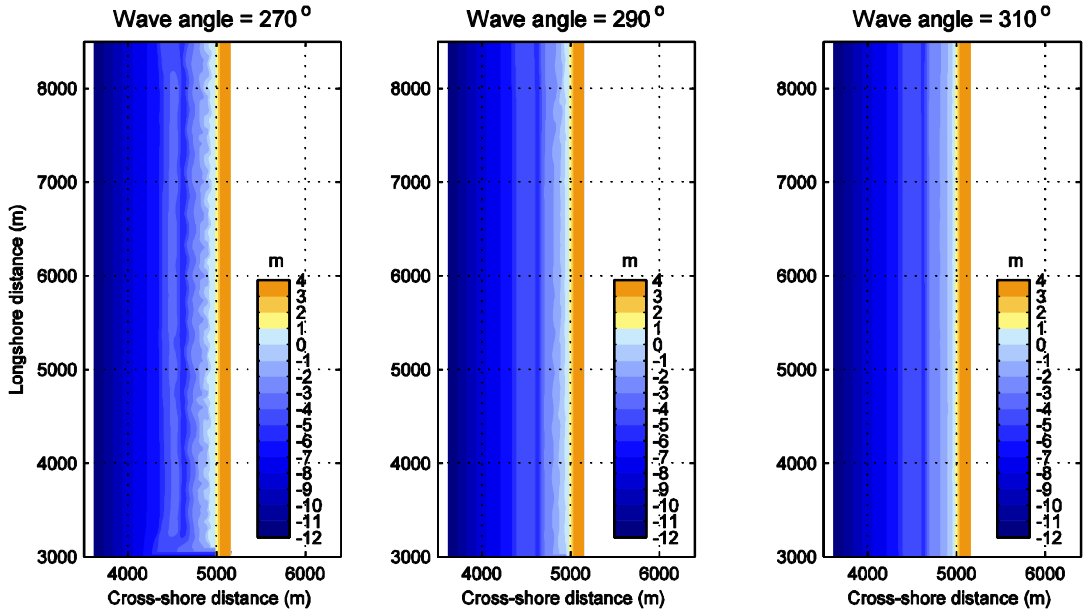

Figure 3.5 *Computed bathymetries with the modified version of Delft-3D, after 10 tidal cycles and for different wave conditions. Wave angle = 270° (left panel), wave angle = 290° (middle panel), wave angle = 310 ° (right panel). Simulations carried out with the modified Delft3D version.*

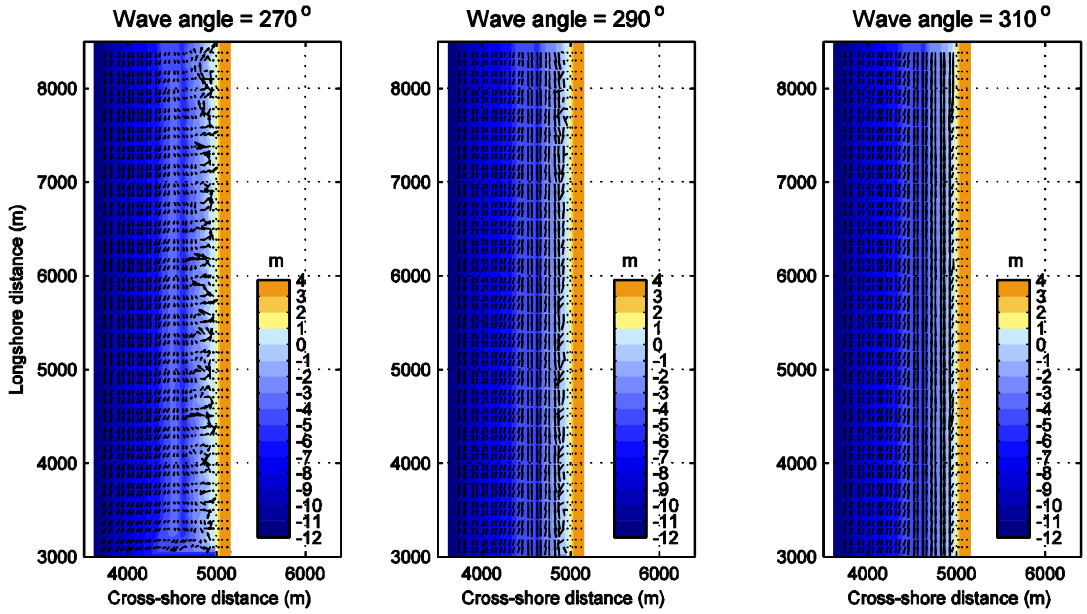

Figure 3.6 *Same as Figure 3.5 , but velocity vectors at the bottom layer, after 10 tidal cycles are added to the final bathymetry. Simulations carried out with the modified Delft3D version.*

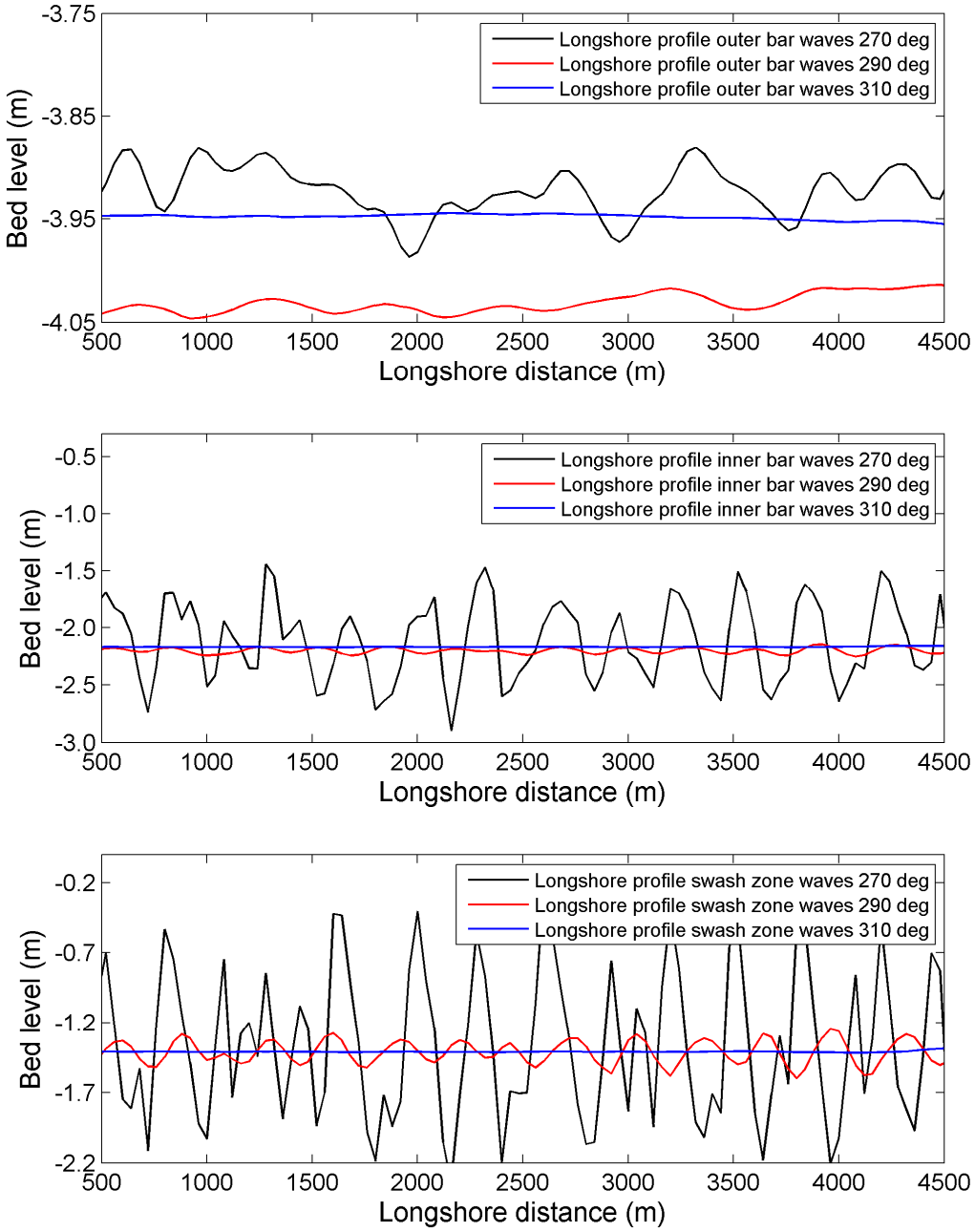

Figure 3.7 *Computed longshore bottom profiles for different wave angles at different cross-shore position: at the outer bar (upper figure), at the inner bar (middle figure) and in the swash zone (lower figure).Simulations carried out with the modified Delft3D version.*

In order to be able to understand the difference in morphodynamics among tests carried out assuming different wave angles and with the two Delft3D versions, significant wave height, cross-shore and longshore velocities were plotted for a cross section in the middle of the domain (Figure 3.8). The following conclusions can be drawn:

- The longshore currents are the dominant hydrodynamic process with respect to tidal currents near the shore. Longshore currents strongly increase when the wave angle increases.
- The longshore currents are more than 0.1 m/s stronger in intensity in the modified Delft3D version than in the standard version. This is related to the different approach of computing shear stresses (Paragraph 2.7.1). As a consequence, the bottom quasi-rhytmic features are smoothed out when the calculation is carried out according to the modified version.
- Average cross-shore currents are negative, due to undertow. Cross-shore currents increase when the wave angle decreases from 310° to 270°. Moreover, they are generally lower in the modified Delft-3D version.
- The cross-shore and longshore currents near the shore (between 4800 m and 5000 m) calculated assuming a 270° angle show a very different behaviour than currents calculated assuming other angles. This is due to the fact that for the 270° case, the quasi-rhythmic bedforms are the dominant feature at the bottom near the shore, leading to the recirculation cells visible in Figure 3.4. The positive (shore-directed) cross-shore current is due to one of these recirculation cells.
- The significant wave height slightly decreases when the wave angle increases from 270° to 310°. The difference in wave height is more evident offshore the outer breaker bar where reaches about 15 cm, reduces between the outer and inner breaker bar, and almost disappear going towards the beach. The difference is related to a discrepancy in the bathymetry evolution between the different tests, and to wave and current interaction effects which modulate the wave height.

In a similar way, the bedload and suspended transport in the cross-shore and alongshore direction, at the central cross section were plotted in Figure 3.9.

In order to help the reader understanding these plots, it is useful to remind how the total load transport is assigned to bedload and suspended load component in Delft3D (Lesser et al., 2004). The bedload component is the result of three different parts:

1) current related bedload transport in the direction of the (Eulerian) near-bed currents

2) wave related bedload transport in the direction of wave propagation

3) wave related suspended transport taking into account wave asymmetry effects.

The suspended load component only includes the effect of currents in an advection-diffusion equation.

Figure 3.9 shows that:

- Suspended transport is dominant with respect to bedload transport.
- Bedload and suspended load in the longshore direction increase with increasing wave angle due to higher longshore currents.
- Suspended load in the cross-shore direction decreases with increasing wave angle due to lower cross-shore currents. In general it is offshore directed due to undertow.
- The tendency of bedload transport in the cross-shore direction is more complex due to the fact that this is affected by the equilibrium between two opposite components: the shore-directed transport due to wave effect, and the offshore-directed transport

due to undertow. Outside the outer breaker bar the bedload transport in cross-shore direction decreases with increasing wave angle, due to the fact that wave height is lower for bigger wave angle. Inside the outer breaker bar, bedload transport in cross-shore direction increases with increasing wave angle due to the fact that the onshore transport do to wave asymmetry becomes relatively more important, with respect to a decrease in undertow effects.

- Bedload in the cross-shore direction, outside the outer bar, is lower in the modified Delft3D version. On the other hand becomes higher onshore the outer bar.
- Bedload and suspended load in the longshore direction are generally enhanced in the modified Delft3D version. This is mainly due to the fact that longshore currents are higher in the modified Delft-3D version.

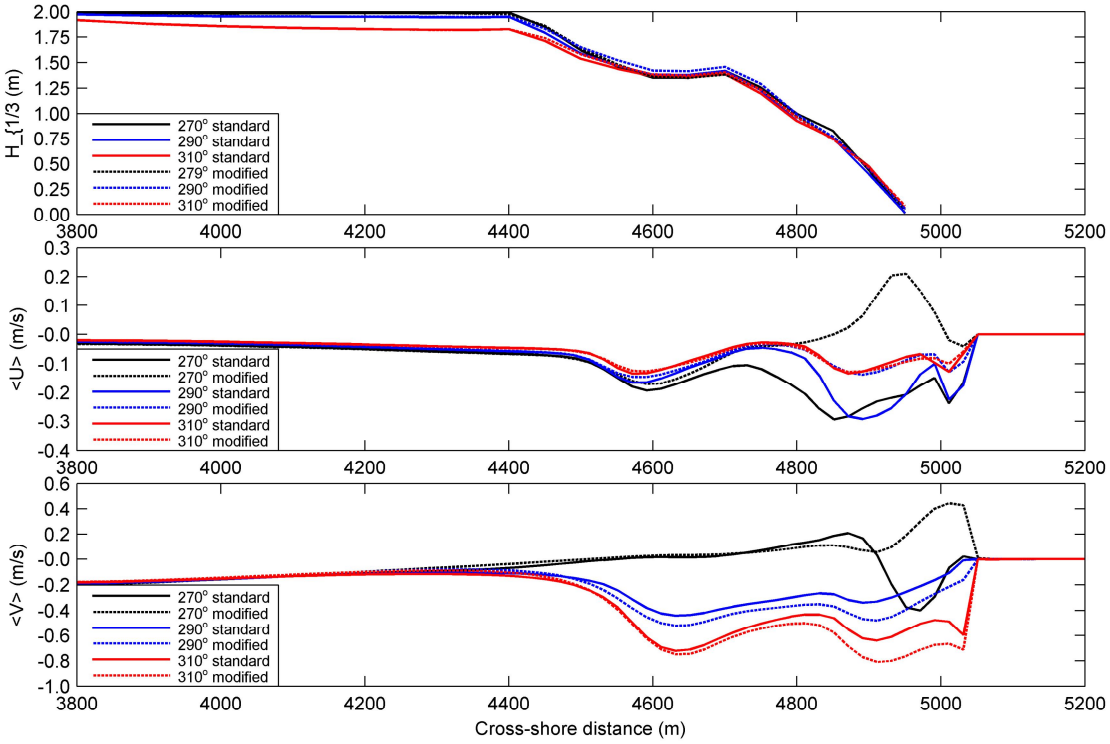

Figure 3.8 *Significant wave height ($H_{1/3}$), depth averaged cross-shore (<U>), and longshore (<V>) velocities along the central cross-shore transect computed for different wave angles, and with the two Delft3D versions. Solid lines represent the output from the standard Delft3D, dashed lines from the modified Delft-3D. All variables were computed at low-tide conditions.*

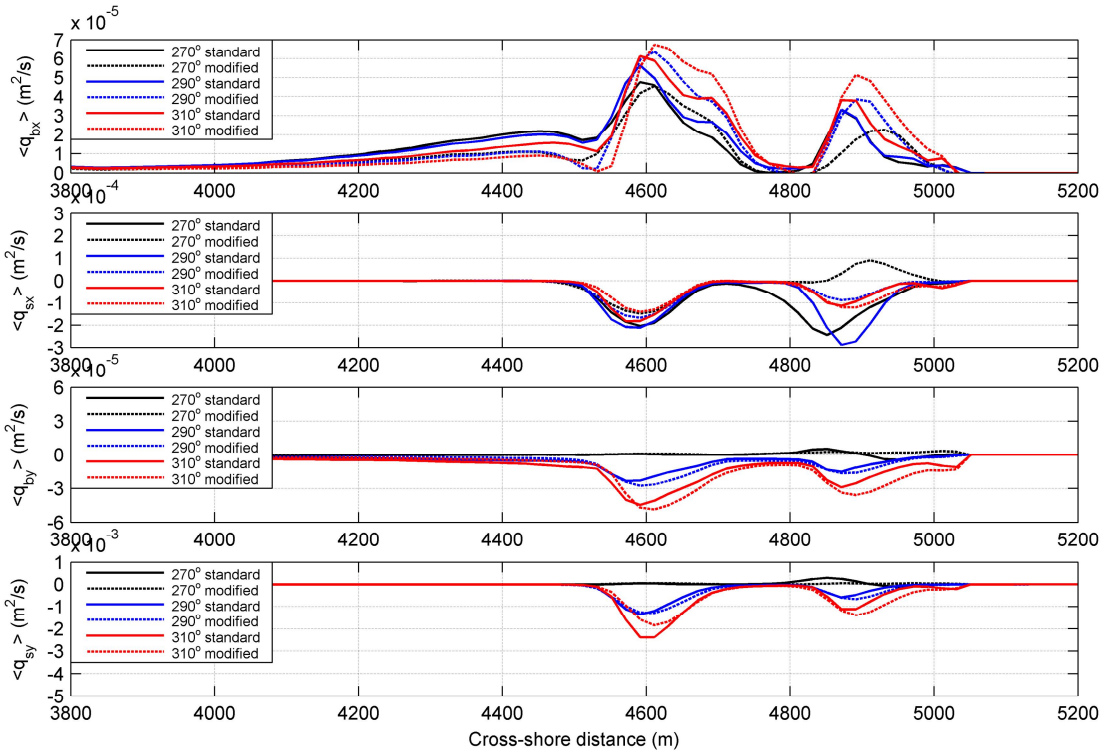

Figure 3.9 *Cross-shore bedload transport (<q_{bx}>), cross-shore suspended load transport (<q_{sx}>), alongshore bedload transport (<q_{by}>, and alongshore suspended load transport (<q_{sy}>) at the central cross section. All variables were computed for different wave angles at low tide conditions. Solid lines represent the output from the standard Delft3D, dashed lines from the modified Delft-3D.*

Discussions and conclusions

Previous modelling experience had shown that longterm morphodynamic simulations could not be carried out due to the formation of quasi-rhythmic features, growing out of control during the simulation. In this Chapter several modification to the standard Delft3D code were tested in order to see whether any improvement to the results could be obtained. Numerical simulations were carried out on a simplified bathymetry and assuming different wave angles in order to show the relative impact of wave and currents on bedform formation.

First of all, tests were carried out with the standard version of the Delft-3D code. Simulations carried out with a wave field approaching the coast perpendicularly have shown the development of the largest quasi-rhythmic bottom features. The growth of these bedforms was related to self organizing properties of the morphodynamic system. Small computation errors provide the initial perturbation responsible to start the positive feedback mechanism between bed and hydrodynamic conditions. These numerical perturbations could be compared to any natural perturbation, which always exist in any system and would provide the growing of features with specific wave lengths. The quasi-rhythmic features tend to increase in wave length and decrease in amplitude, when the angle of wave approach increases. For an angle of about 40° these features completely disappear. This behaviour was related to a gradually increase of the longshore component of the velocity currents, which tend to contrast the formation of vortex and rip currents.

Despite the fact that longshore bedforms are a feature existing in nature and whose growth can be represented by numerical calculations, the output from the standard Delft3D code showed the formation of bedforms of too large amplitude which grow from the coastline up to the offshore bar. Therefore, the same tests were repeated including a number of modifications to the standard Delft3D code. Result of these modifications is an increase in the longshore currents and a decrease in the undertow component in cross-shore direction. As a consequence, quasi-rhythmic feature still develop but with a reduced amplitude and only along the coastline. These results look at first view more realistic than what was previously obtained as output of the standard Delft3D. However, further work need to be carried out in order to validate these results, comparing them with hydrodynamics measurements coupled to morphodynamics surveys.

4 Test case 2: shoreface nourishment scenario

4.1 Introduction

In this chapter the (relative) impact of a shoreface nourishment on the nearshore morphology as simulated by the standard and adjusted Delft3D version is intercompared. With the model set-up as described in Chapter 2, one year of morphological evolution of the longshore uniform bathymetry representative for the Egmond region is simulated. Wave climate is schematized through four wave conditions. In order to make sure that the modelled results are, to large extents, not influenced by the order of the four wave conditions, the same simulation was carried out changing the wave condition order (Section 4.2).

The unnourished situation is the reference for studying the impact of the nourishment. A schematized nourishment is then added to the reference situation. The shoreface nourishment has a volume of 400 m^3 per meter coast with a longshore length of 2 km, corresponding to a total nourishment volume of $0.8*10^6$ m^3. The seaward slope of the nourishments has been set to 1:10 and the top of the nourishments is located at a water depth of 5 m. These values correspond to a typical Dutch shoreface nourishment. In Walstra et al. (2004) this shoreface nourishment scenario is referred to as nourishment design 2. Figure 4.1 shows the 2D morphology of the reference situation, the shoreface nourishment and the difference between these two (in metres). Figure 4.2 shows the cross-shore morphology of the transect in the middle of the (location of the) nourishment.

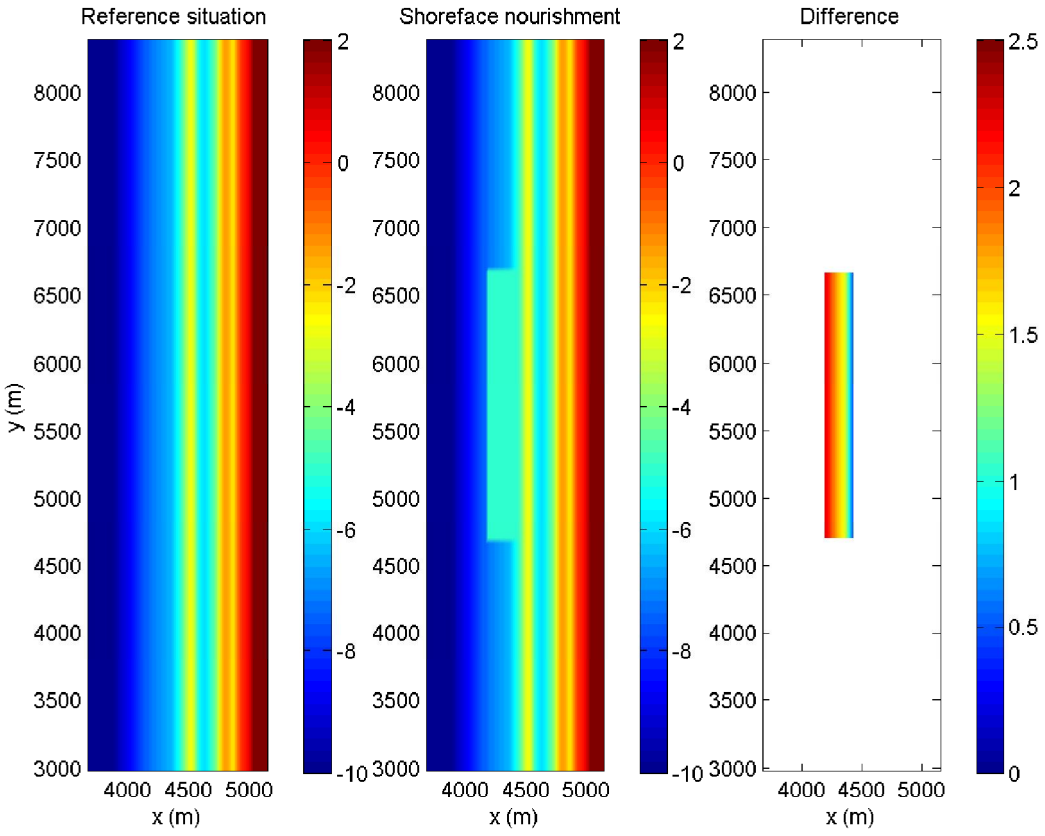

Figure 4.1 2D morphology (in meters) of the reference situation, the shoreface nourishment and the difference between these two (nourished – reference situation).

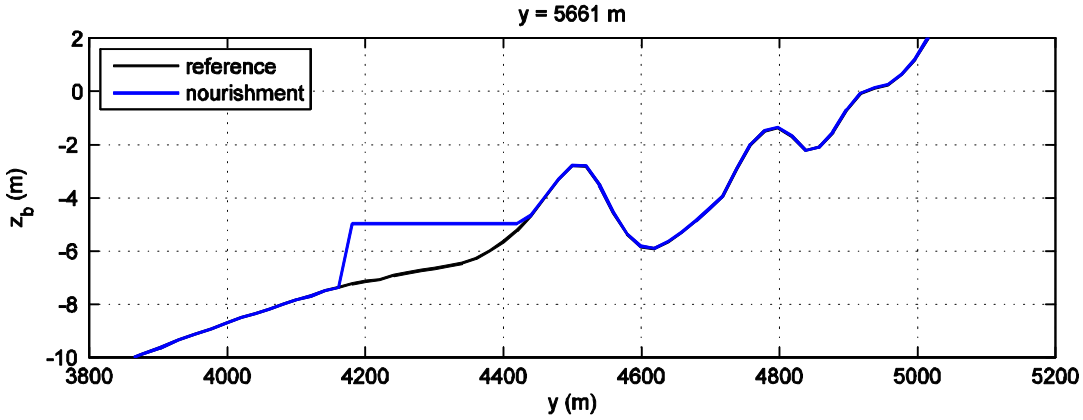

Figure 4.2 *Cross-shore morphology of the transect in the middle of the (location of the) nourishment.*

The model simulation results are qualitatively intercompared with what is considered to be the general morphodynamic response of the Dutch coastal system to a shoreface nourishment, which is described in Section 4.3. Section 4.4 presents the morphological evolution of the reference situation and the nourished case, computed by the standard Delft3D version. The (relative) morphological impact of the shoreface nourishment is assessed and the observed morphological developments are explained by studying the wave, flow and sand transport processes.

The same simulations are then repeated for the adjusted Delft3D model, presented in Section 2.7, in order to see eventual changes to the modelled results (Section 4.5).

4.2 Influence of wave order schematization

As shown in Paragraph 2.5.2, wave forcing at the boundary was schematized by means of four wave conditions. In this Paragraph, the influence of the wave condition order on the morphodynamic evolution is assessed.

Two morphodynamic simulations were carried out forced by the same wave conditions at the boundary, but with different order. In Table 4.1 waves are schematized according to the "standard order", which corresponds to the wave schematization described in Paragraph 2.5.2, and to the "modified order". If the order on which waves are schematized has no impact on the morphodynamics, as would be desired, the same bottom profile will be obtained at the end of the two simulations.

Table 4.1 *Morphological wave conditions. On the left hand side of the table, wave conditions are schematized following the "standard order" (Table 2.2). On the right hand side of the table, wave conditions are schematized following a different order.*

Condition	Standard order				Modified order			
	Hs (m)	Tp (s)	Direction (° N)	Morfac	Hs (m)	Tp (s)	Direction (° N)	Morfac
1	2.75	8.3	217	11.142	1.25	6.3	217	127.84
2	1.25	6.3	217	127.84	2.75	8.3	217	11.142
3	2.75	9.5	317	8.83	1.25	6.3	317	91.04
4	1.25	6.3	317	91.04	2.75	9.5	317	8.83

In Figure 4.3, the influence of wave order schematization on the cross-shore profile is shown. The Figure shows that the effect of wave order schematization on the final morphology is limited, since the two profiles at the end of the simulations (after 1 year) are very similar (Figure 4.3 (d)). Both profiles show an offshore migration and smoothing of the two bars. However, some difference can be seen comparing the two profiles. The main reason behind this difference is due to the fact that most of the morphodynamic changes occur after the first wave condition (Figure 4.3 (a)). The first wave condition, when waves are schematized following the standard order, is represented by a very energetic wave condition (Hs = 2.75 m), which leads to a net offshore migration and smoothening of the bars due to a strong return flow. On the other hand, the first wave condition in the modified order schematization is represented by a relative mild wave (Hs = 1.25 m), which leads to a onshore migration and smoothening of the bars. Even the energetic wave state of condition 2, in the modified order schematization (Hs = 2.75 m), is not sufficient to generate the same profile as the one given by the standard wave condition (Figure 4.3 (b)).

However, we can conclude that the effects of the wave order schematization on the morphodynamics are relative small. Therefore, also the relative errors due to order schematization on the final modelled bathymetry are limited. Therefore, we will choose the standard order to drive the morphodynamics computations included in this Chapter.

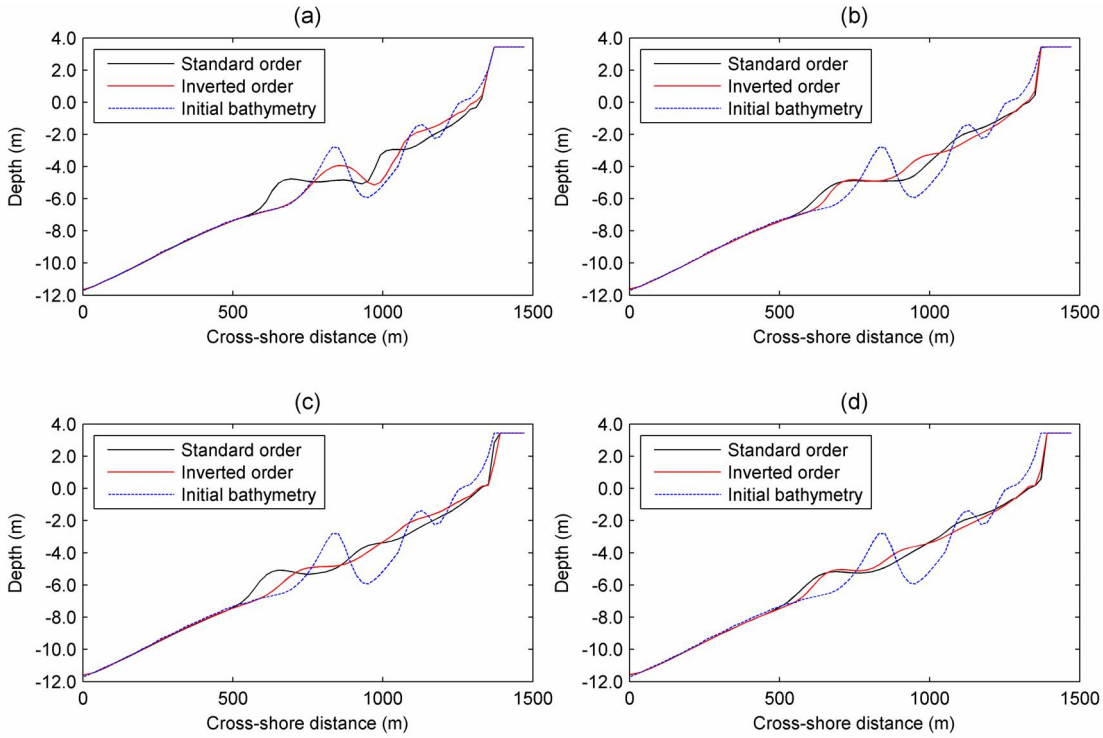

Figure 4.3 *Influence of wave order schematization on the cross-shore morphodynamic evolution. All profiles refer to a section with longshore position equal to 4961 m. The blue dashed line represents the initial bathymetry, the black line represents the profile after each wave condition and following the standard order for the wave schematization, the red line represents the profile after each wave condition when the wave order is schematized with a different order.(a) cross-shore profile after wave condition 1; (b) cross-shore profile after wave condition 2; (c) cross-shore profile after wave condition 3; (d) cross-shore profile after wave condition 4.*

4.3 General morphodynamic response to a shoreface nourishment

The following suggestions are taken from Baptist et al. (2009) and based on reports and articles by Kroon et al. (1994), Hoekstra et al. (1996), Van Duin et al. (2004), Grunnet et al. (2004), Cohen & Brière (2007), Ojeda et al. (2008) and Walstra et al. (2008). These are both model and data analysis studies.

A shoreface nourishment has the following two effects on the coastal system.

1. The lee effect. The artificial sand bar increases wave dissipation, by which the wave height and longshore current onshore of the nourishment decrease. As a result, the longshore sand transport capacity decreases here and therefore sand accumulates upstream and erodes downstream. If the waves approach shore normal, the leeside of the nourishment possibly erodes as a result of divergence of longshore currents induced by longshore differences in wave set-up.
2. The feeder effect. This refers to the feeding of coastal system onshore of the nourishment with nourished sand due to cross-shore sand transport processes. The net sand transport in onshore direction is enhanced by the nourishments, because, i) seaward suspended load decreases because the additional wave dissipation by the nourishments reduces the offshore-direction undertow and the wave-induced sediment suspension ii) onshore bed- and suspended load increase at the nourishment due to additional wave skewness related to the lower water depth compared to the unnourished case.

Furthermore, the shoreface nourishment affects the autonomous behaviour of the breaker bars. The autonomous behaviour of the breaker bars is periodically and consists of the following phases: 1) generation near the beach, 2) net migration in seaward direction through the surf zone, and 3) de-generation at the edge of the surf zone. The latter phase triggers the generation of a new breaker bar (phase 1) and the seaward migration of the now outer breaker bar (phase 2). This cycle is a cross-shore distribution of sand without a significant loss in offshore direction. The number of breaker bars (between 0 and 4) and the duration of this cycle (between 0 and 15 years) vary along the Dutch coast and are, among other things, dependent on the steepness of the coastal profile.

The nourishment, placed against the outer breaker, generally re-shapes itself relatively quickly (within a few months) into a bar with a landward trough. As a result of this, the offshore migration of the original breaker bars is halted; sometimes they even start migrating in the onshore direction. During this stop of offshore bar migration, the bars keep their pre-nourished dimensions.

The above-described effects of a shoreface nourishment are temporary, as the volume of a nourishment decreases in time. The duration of the impact of a nourishment is related to its lifetime, which lies between the 2 and 8 years for the shoreface nourishments studied in The Netherlands. The lifetime is, among other things, dependent on the nourishment volume, the grain size, longshore nourishment length and the location of the nourishment.

4.4 Simulations with the standard Delft3D version

Figure 4.4 shows the initial bathymetry, the bathymetry after 1 year computed with the standard Delft3D version and the difference between these two. Figure 4.5 shows the cross-

shore morphology of the central transect (at *y* = 5661 m) after each of the four wave conditions described in Section 2.5.

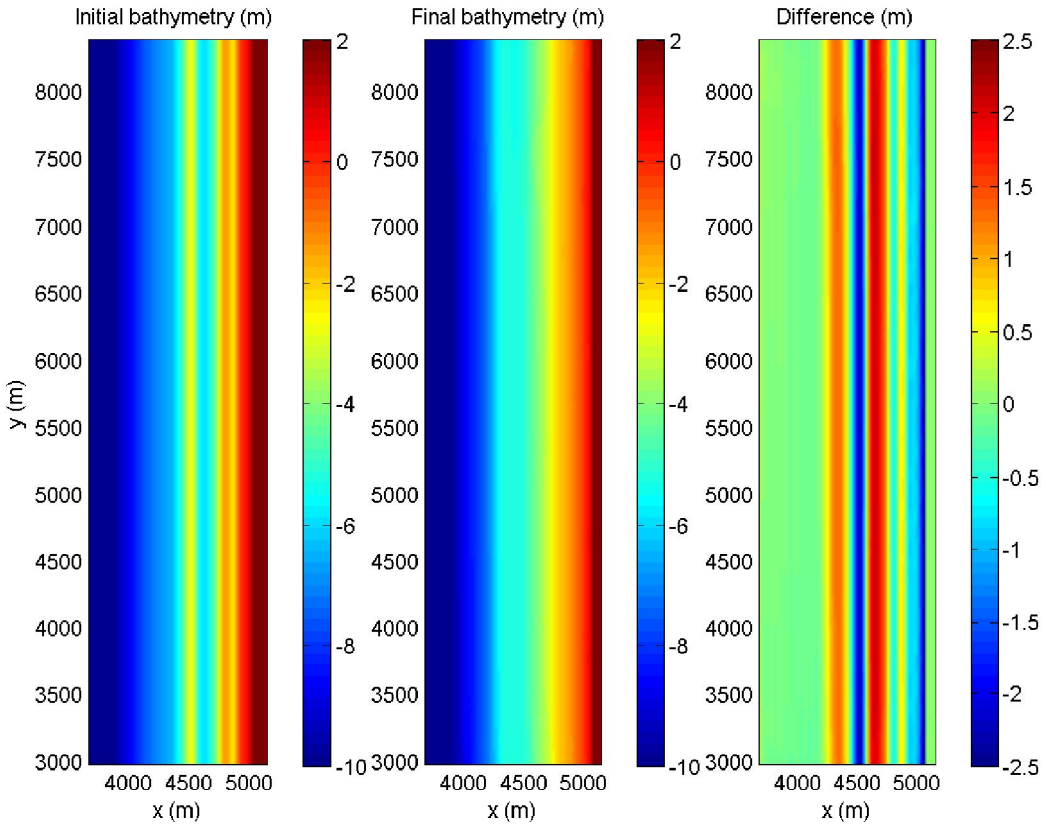

Figure 4.4 *Initial bathymetry, final bathymetry and difference between these two (final – initial) for the reference case as computed by the standard Delft3D version.*

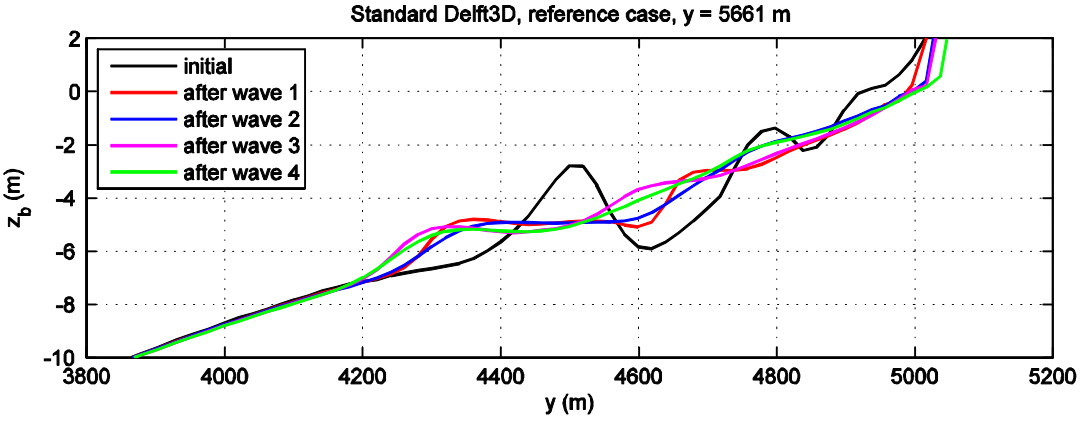

Figure 4.5 *Development of the cross-shore profile at y = 5661 m. Reference case; computed by the standard Delft3D version.*

The simulations with the standard Delft3D version as plotted in Figure 4.4 and Figure 4.5 show that the breaker bars and the swash bar flatten considerably, and that the breaker bars

migrate a few hundred metres in the offshore direction. Furthermore, the upper part of the profile (between $x \approx 4900$ and 5000 m) shows significant erosion. After 1 year of computation, only the outer breaker bar can still clearly be observed. The largest morphological changes are associated with wave condition 1 where H_s = 2.75 m, T_P = 8.3 s and $\theta = 217^o$ (from the Southwest). During the next, milder wave condition (H_s = 1.25 m and T_P = 6.3 s) from the same direction, the breaker bars migrate in the onshore direction, especially the inner breaker bar. The next large wave condition (H_s = 2.75 m, T_P = 9.5 s, $\theta = 317^o$) induces offshore bar migration again, followed by slightly onshore bar migration during the final wave condition (H_s = 1.25 m, T_P = 6.3 s, $\theta = 317^o$) and a flattening of the inner bar. The model is thus able to reproduce the offshore bar migration during severe wave conditions and onshore bar migration during milder wave conditions as typically observed in the field and laboratory (see e.g. Arcilla et al, 1994). However, the considerable flattening of the bars seems to be unrealistic and needs further attention.

Figure 4.6 shows the initial bathymetry, final bathymetry and the difference between these two for the shoreface nourishment. Figure 4.7 shows the initial and final relative impact of the nourishment, i.e. the difference between the bathymetries for the nourished and unnourished case. Figure 4.8 shows the morphological development of three different cross-shore transects: (i) 500 m north of the nourishment, (ii) in the middle of the nourishment and (iii) 500 m south of the nourishment.

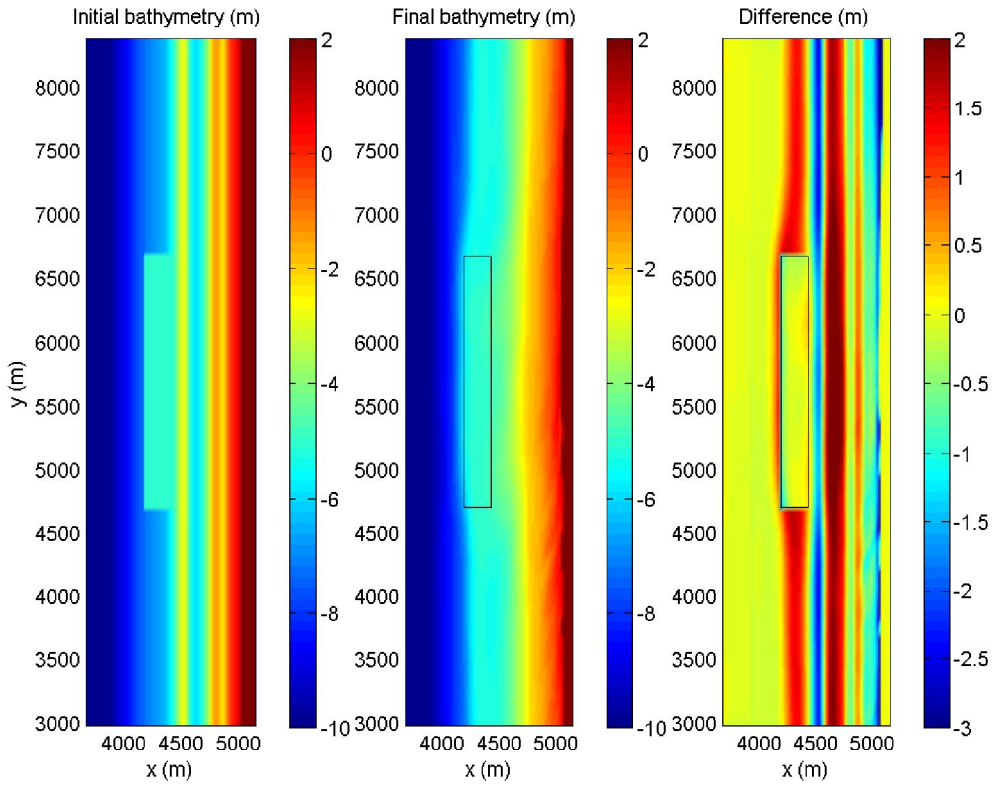

Figure 4.6 *Initial bathymetry, final bathymetry and difference between these two (final – initial) for the shoreface nourishment as computed by the standard Delft3D version. The black lines denote the contours of the nourishment.*

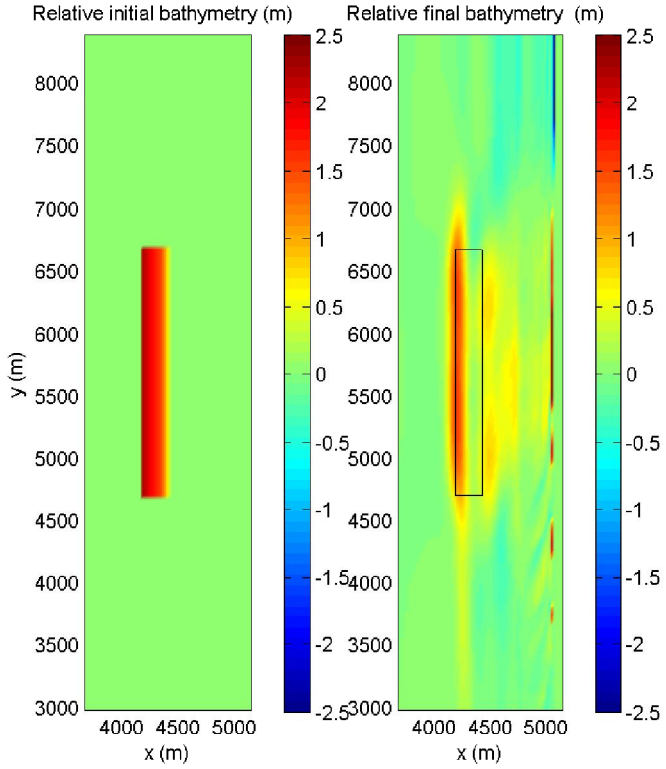

Figure 4.7 *Difference between the initial bathymetry with and without a nourishment (left panel) and difference between the final bathymetry with and without a nourishment (right panel). The black lines denote the contours of the nourishment. Computed by the standard Delft3D version.*

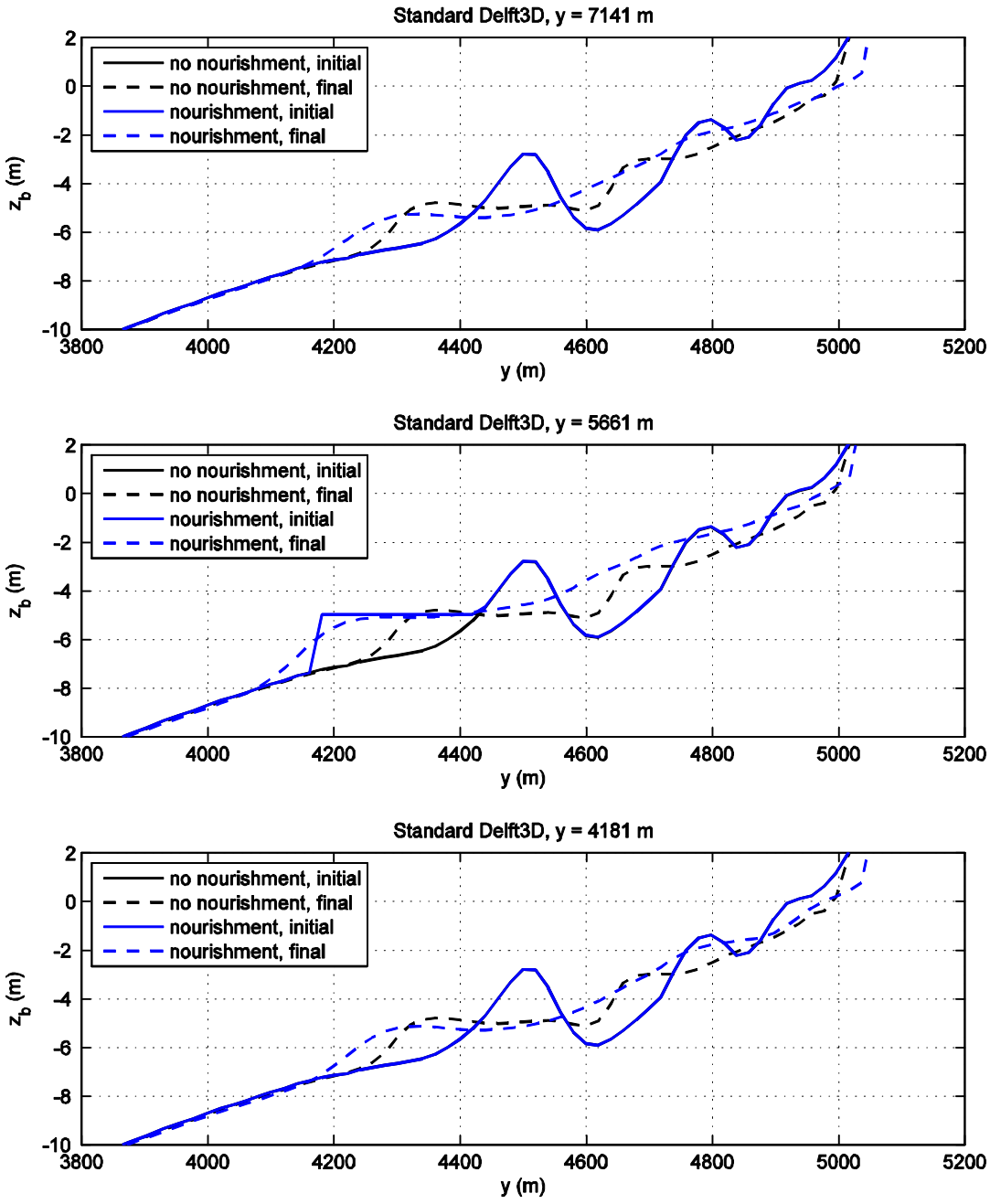

Figure 4.8 *Development of the cross-shore profile at different transects. Upper panel: 500 m north of nourishment, middle panel: centre of nourishment, lower panel: 500 south of nourishment. Computed by the standard Delft3D version.*

From these figures we can conclude the followings:

- After one year, the impact of the shoreface nourishment can still clearly be observed, especially at the offshore part of the nourished section. The nourished sand has diffused partly in the offshore and longshore directions, but most of the sand is transported in the onshore direction.
- The nourishment does not display longshore migration.

- The shoreface nourishment and the outer breaker bar merge into a large and flat bar with its crest a few hundred metres offshore of the original outer breaker bar. The inner bar flattens so much that it can hardly be identified as a bar, and moves in the onshore direction.
- Surprisingly, the outer breaker bars at the transects 500 north and south of the nourishment are more offshore located for the nourished case.
- The upper part of the cross-shore profiles (shoreward of the outer breaker bar) benefits most from the nourishments. The effect is stronger in the centre of the nourishment, but 500 m north and south of the nourishments this can still be clearly observed.
- The (partly) dry part of the cross-shore profile experiences strong erosion in the nourished case compared to the unnourished case. This is probably not realistic and due to inadequacy of the model to simulate the transition from the wet to the dry part of the beach correctly. Moreover, it is likely to be related to an inappropriate spatial grain size distribution, assumed to be constant over the whole area.

To investigate why these morphological changes occur, we investigate the wave dynamics, hydrodynamics and sand dynamics. We focus on wave condition 1, the central cross-shore transect and two instances during the tidal cycle: (near) low tide and high tide. These instances occur 4.5 and 8.5 hrs after the start of the morphological computation, respectively. The water level at the offshore boundary of the central transect is ≈ -0.6 m at low tide and ≈ +1.0 m at high tide. Figure 4.9 shows the root-mean-square wave height (H_{rms}), the depth-averaged cross-shore current velocity ($|U|$), the depth-averaged longshore current velocity ($|V|$), and the bed level along the central cross-shore transect. We distinguish between low tide (solid lines) and high tide (dashed lines) and the nourished case (black lines) and the unnourished case (blue lines). In a similar way the bedload and suspended load in cross- and longshore direction are presented in Figure 4.10.

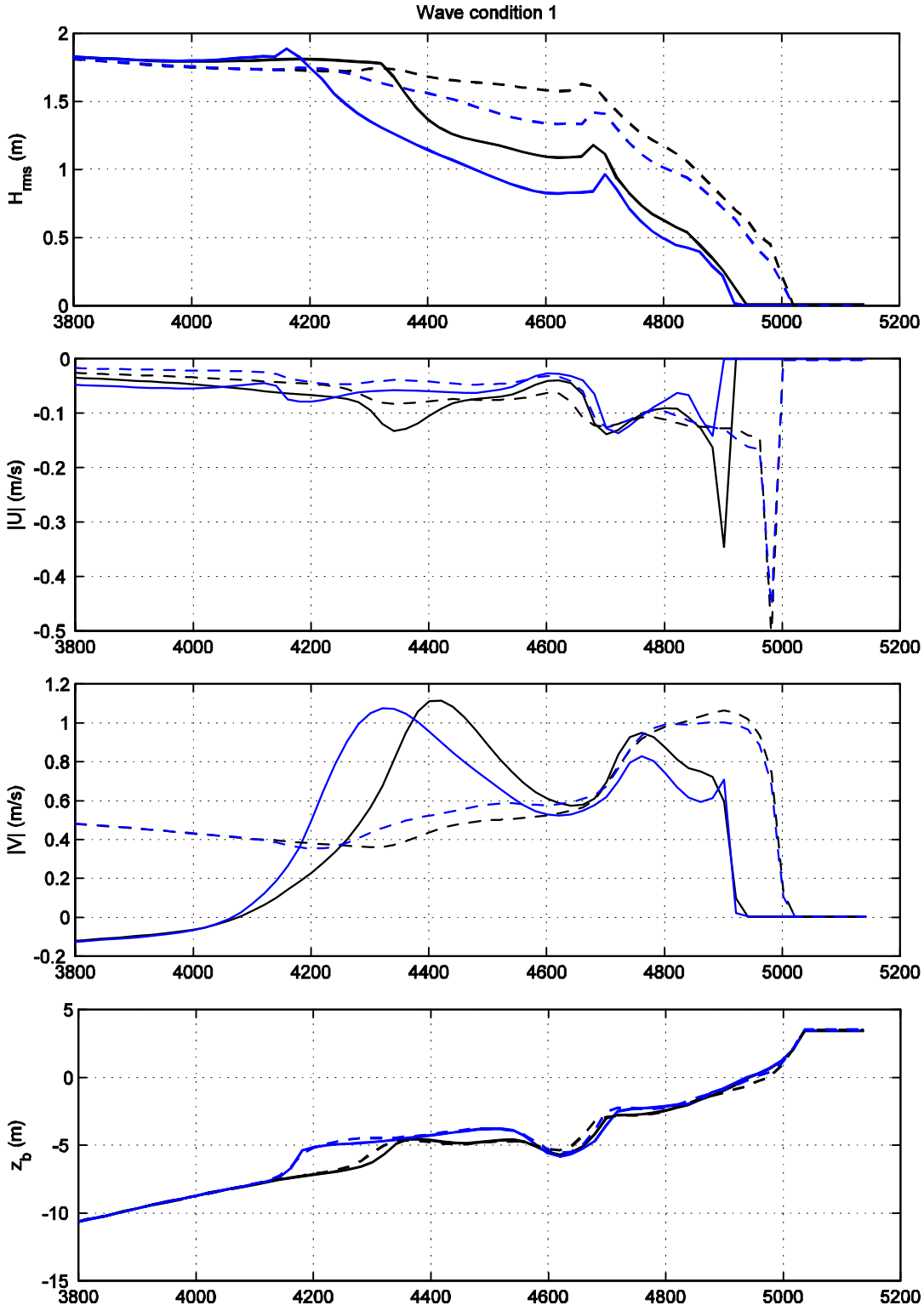

Figure 4.9 *Root-mean-square wave height, depth-averaged cross-shore and longshore current velocity and bed level along the central cross-shore transect. Black lines: without nourishment, blue lines: with nourishment, solid lines: at low tide, dashed lines: at high tide. Computed by the standard Delft3D version.*

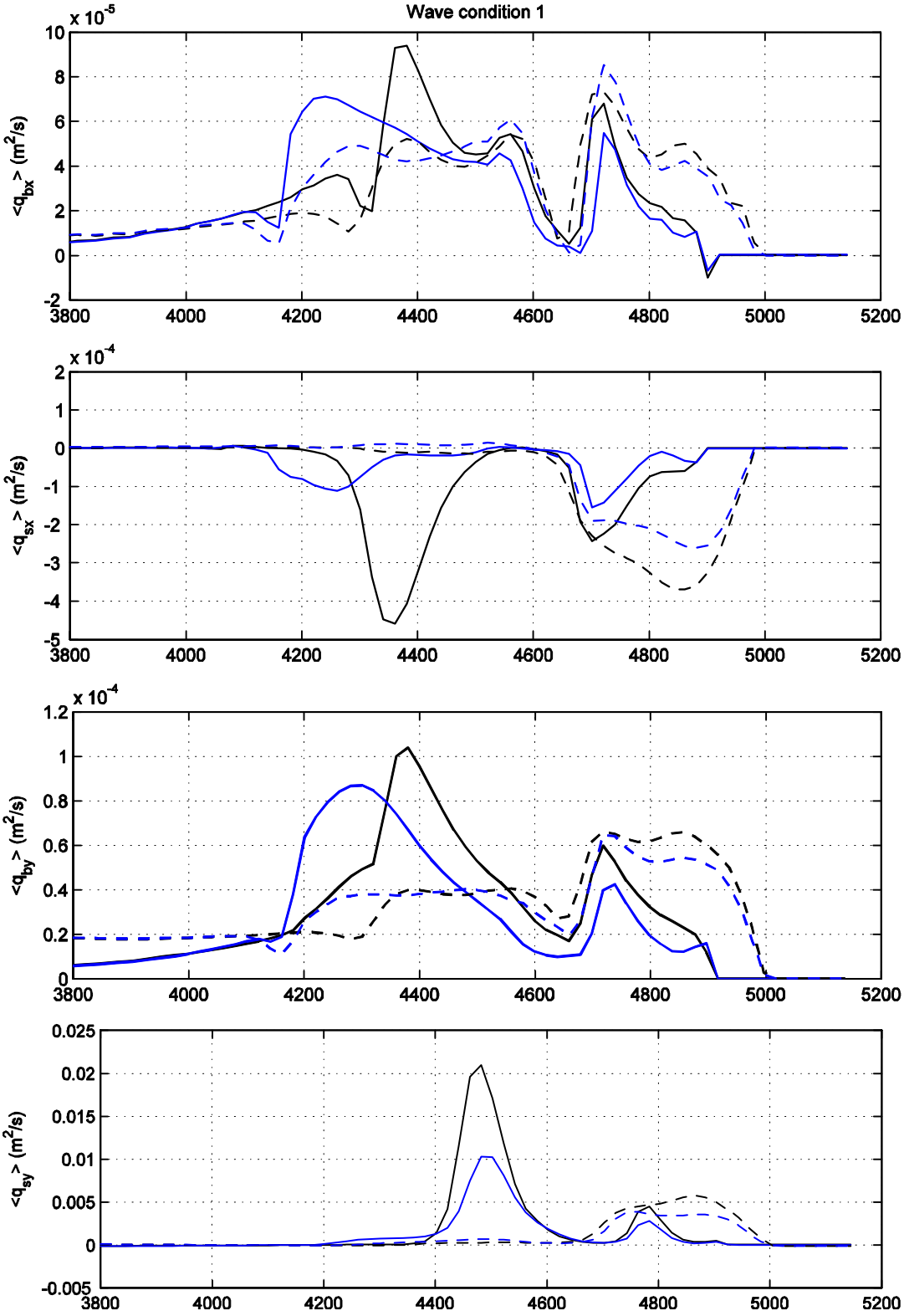

Figure 4.10 *Cross-shore and longshore bedload and suspended load along the central cross-shore transect. Black lines: without nourishment, blue lines: with nourishment, solid lines: at low tide, dashed lines: at high tide. Computed by the standard Delft3D version.*

These figures show that the nourishment strongly reduces the wave height at the location as well as onshore of the nourishment due to relatively more breaker-induced wave energy dissipation related to the relatively lower water depth. This is true except for the most offshore section of the nourishment (between $x \approx 4100$ and 4200 m) where a small increase in wave height can be observed (of the order of cm's) due to relatively more wave shoaling. The effect of the nourishment on the wave height is strongest at low tide, because the water level is lowest then and, as a consequence, the relative reduction of the water depth due to the nourishment highest. The wave height reduction at low tide reaches a maximum of almost 0.5 m slightly offshore of the middle of the newly-formed large and flat outer breaker bar (at $x \approx$ 4300 m). At high tide, the maximum wave height reduction induced by the nourishment is about 0.3 m and occurs more onshore (compared to at low tide) near the crest of the inner breaker bar.

The negative (offshore-directed) depth-averaged cross-shore current is a compensating flow for the onshore-directed mass flux near the surface (Stokes' drift and induced by wave breaking). In the Delft3D formulations the onshore-directed mass flux (and hence the compensating return flow) is proportional to the short wave energy, the roller energy and the cosine of the wave angle, and inversely proportional to the wave celerity (Reniers et al., 2004). This explains the high correlation between the cross-shore behaviour of the wave height and the depth-averaged cross-shore currents as well as the fact that these currents at the location off- and onshore of the nourished section are lower than for the unnourished case. The depth-averaged longshore currents are driven by wave- and roller-induced forces related to radiation stress gradients. As the point of wave breaking (at low tide) is shifted seaward due to the nourishments, so is the location of the longshore current maximum. Therefore, also the longshore currents shoreward of the nourishment are somewhat lower in the nourished case. During high tide, the differences between the longshore currents for the nourished and unnourished case are not that large.

Before discussing the sand transport processes, it is important to realize that the bedload and suspended load contain current- and wave-related components (Section 3.5). In cross-shore direction the current-related bedload and suspended load are generally offshore-directed due to the negative undertow. The wave-related transport is generated by wave skewness (relatively high onshore orbital velocities and relatively low offshore orbital velocities) and therefore in the direction of wave advance, so containing a cross-shore and longshore component depending on the wave angle. This means that the net transport in cross-shore direction is positive (onshore) if wave-related transport is dominant and negative (offshore) is current-related transport is dominant. The suspended load in longshore direction is driven by the wave-driven longshore current, which is for wave condition 1 directed to the North.

The plots of the sand transport show that the suspended load in the surf zone is 1-2 orders of magnitude larger than the bedload. The cross-shore distributions of the transport components resemble those of the currents, but the impact of the nourishment is more apparent on the suspended transport. At the seaward side of the nourishment, the onshore transport components are enhanced in the nourished case, as the wave skewness is larger related to the smaller water depth. Shoreward from here, this effect becomes smaller and is counteracted by the reduced wave height resulting in smaller onshore bedload. The increasingly onshore transport due the shoreface nourishment is called the "feeder effect" in literature (see e.g. Grunnet et al., 2004).

The “lee effect” refers to the ability of the nourishment in increasing wave dissipation with a corresponding shoreward reduction in longshore current velocities leading to increased deposition of sediment carried along with this current (Grunnet et al., 2004). Figure 4.11 clearly illustrates the lee effect. It shows the cross-shore distribution of the total longshore sand transport for three different cross-shore transects: 500 m south of the lower contour of the nourishment, in the centre of the nourishment and 500 m north of the upper contour of the nourishment; at low tide for wave condition 1. The upper panel corresponds to the unnourished case, the lower panel to the nourished case. For the unnourished case there is hardly any longshore gradient in the longshore transport rate. For the nourished case the longshore transport rates south of the nourishment are hardly affected by the nourishment. However, the longshore transport rates in the lee of the nourishment are reduced significantly, which results in sand accumulation here. The longshore transport rates 500 m north of the northern contour of the nourishment are also very much affected.

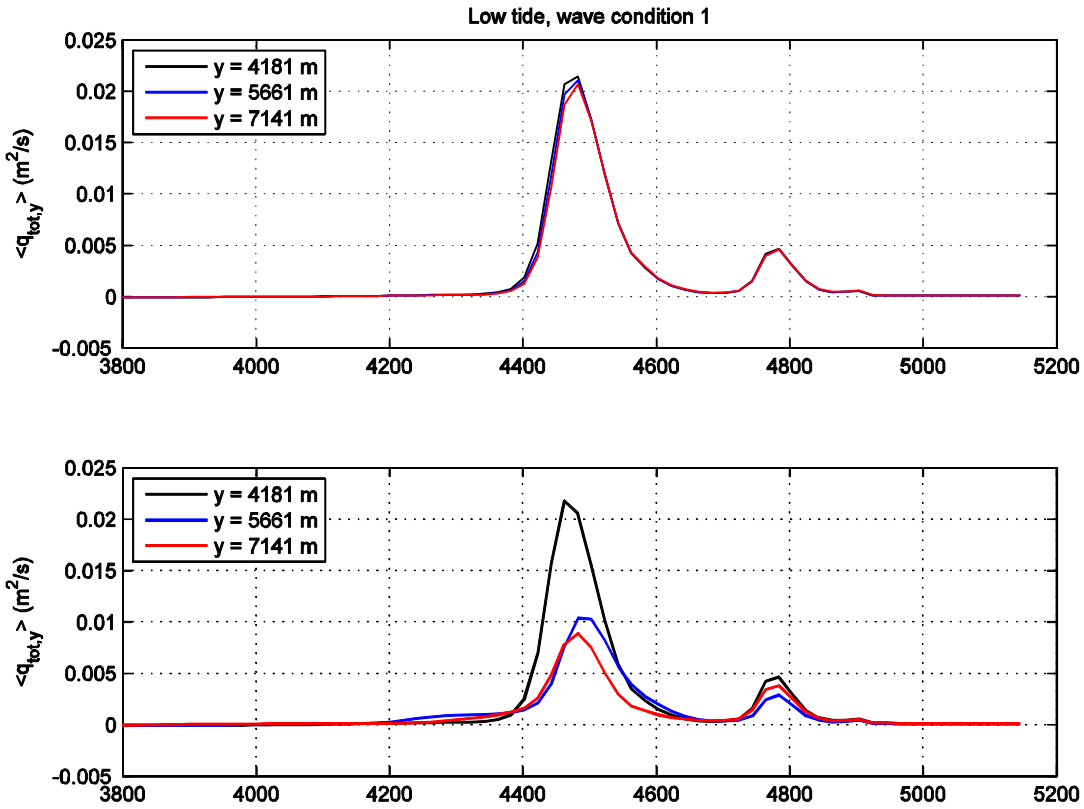

Figure 4.11 *Cross-shore distribution of the total load in longshore direction at low tide for three different cross-shore transects. Upper panel: unnourished case, lower panel: nourished case. Computed by the standard Delft3D version.*

4.5 Simulations with the adjusted Delft3D version

The same simulation shown in Section 4.4 with a shoreface nourishment placed at the outer bar, was repeated adopting the modified Delft3D version, including the modifications described in Section 2.7.

Figure 4.12 shows the morphological development of the shoreface nourishment as computed by the adjusted Delft3D version. Figure 4.13 and Figure 4.14 intercompare the simulations with the standard and adjusted Delft3D model. Figure 4.13 shows the 2D morphology, Figure 4.14 the morphological development of the central, northern and southern cross-shore transect. These figures show that the two Delft3D versions compute qualitatively the same morphological evolution of the nourishment. However, the following differences can be observed:

- The adjusted Delft3D version computes less off-shore migration of the bar South and North of the nourishment.
- For both versions a high unrealistic erosion at the shore line is observed, particularly south and north of the nourishment.

To explain these differences in the computed morphology between the two versions, the wave, flow and sand transport phenomena at low and high tide for wave condition 1 have been analyzed.

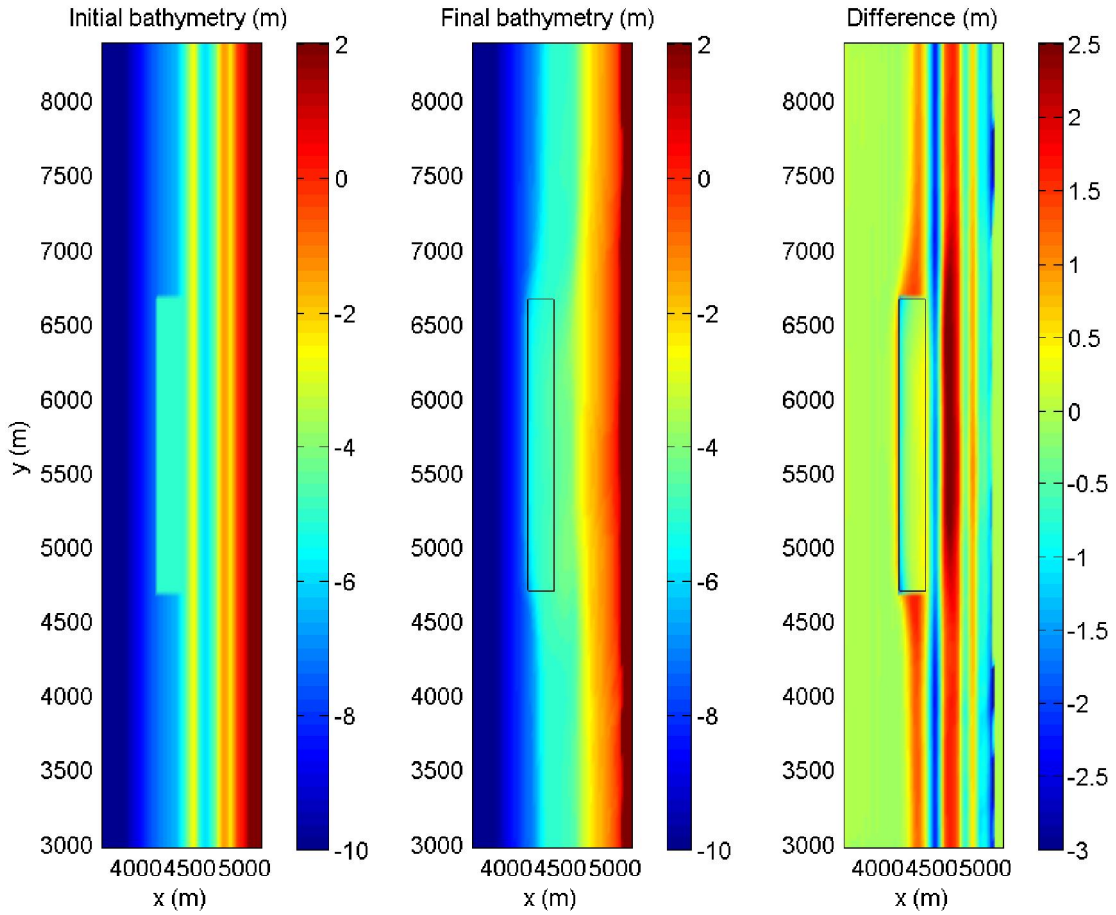

Figure 4.12 *Initial bathymetry, final bathymetry and difference between these two (final – initial) for the shoreface nourishment as computed by the adjusted Delft3D version. The black lines denote the contours of the nourishment.*

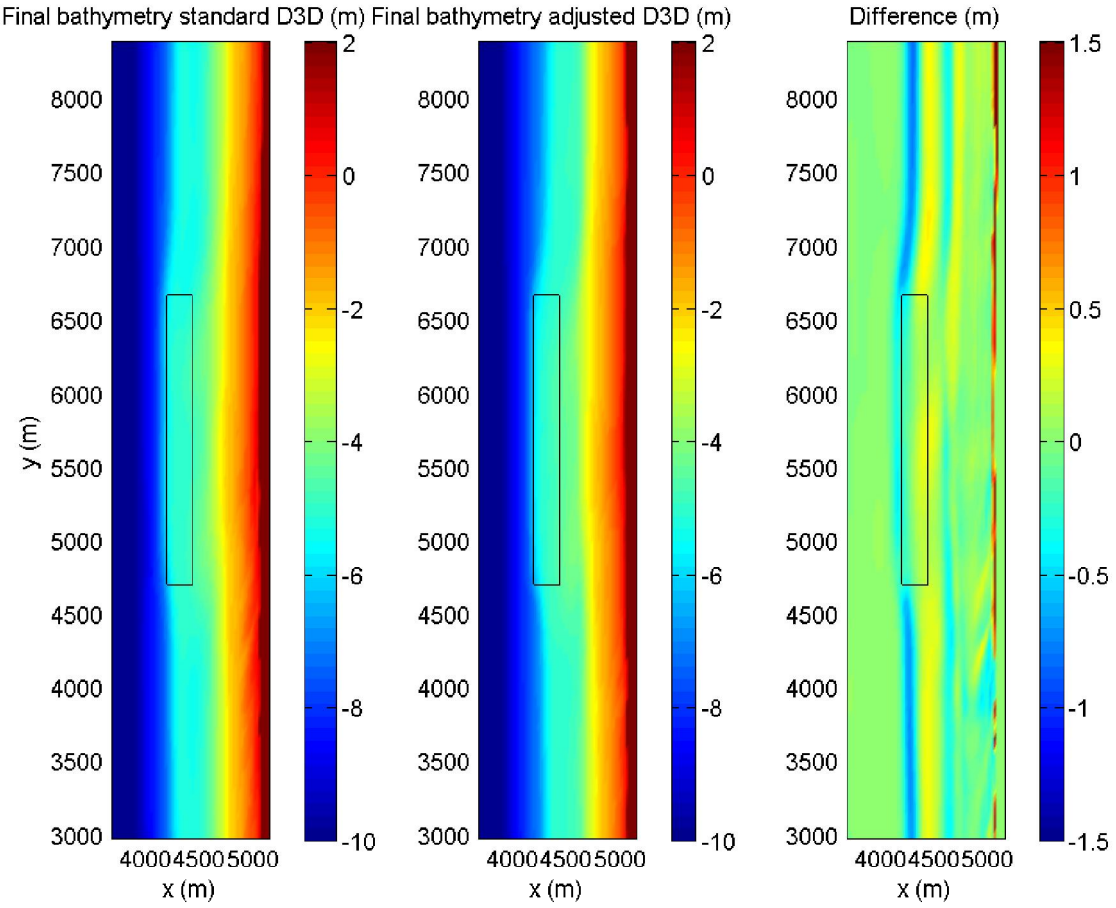

Figure 4.13 *Final bathymetry for the shoreface nourishment as computed by the standard and adjusted Delft3D version, and the difference between these two (adjusted – standard). The black lines denote the contours of the nourishment.*

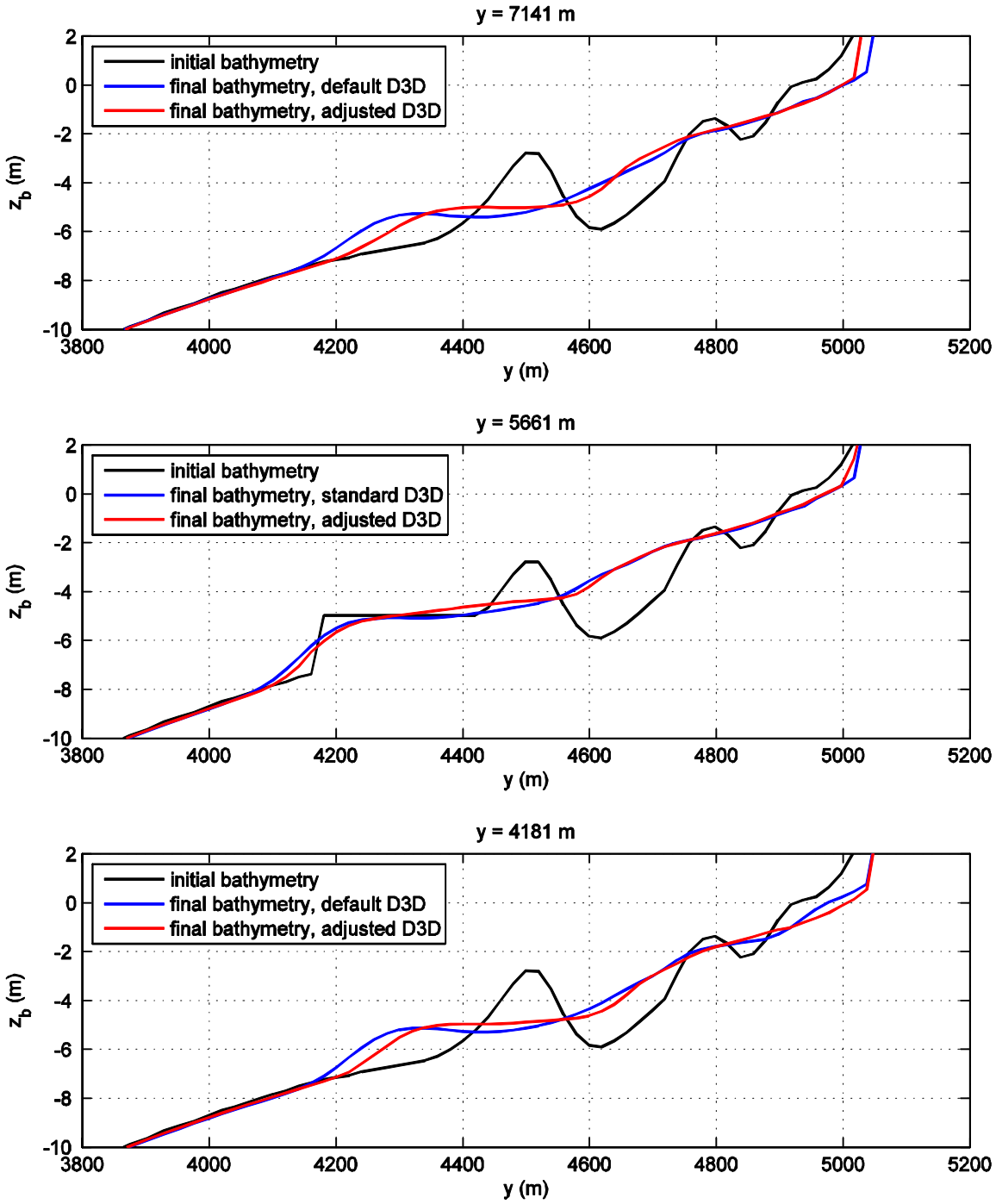

Figure 4.14 *Development of the cross-shore profile at different transects; top: 500 m north of nourishment; middle: centre of nourishment; bottom: 500 south of nourishment.*

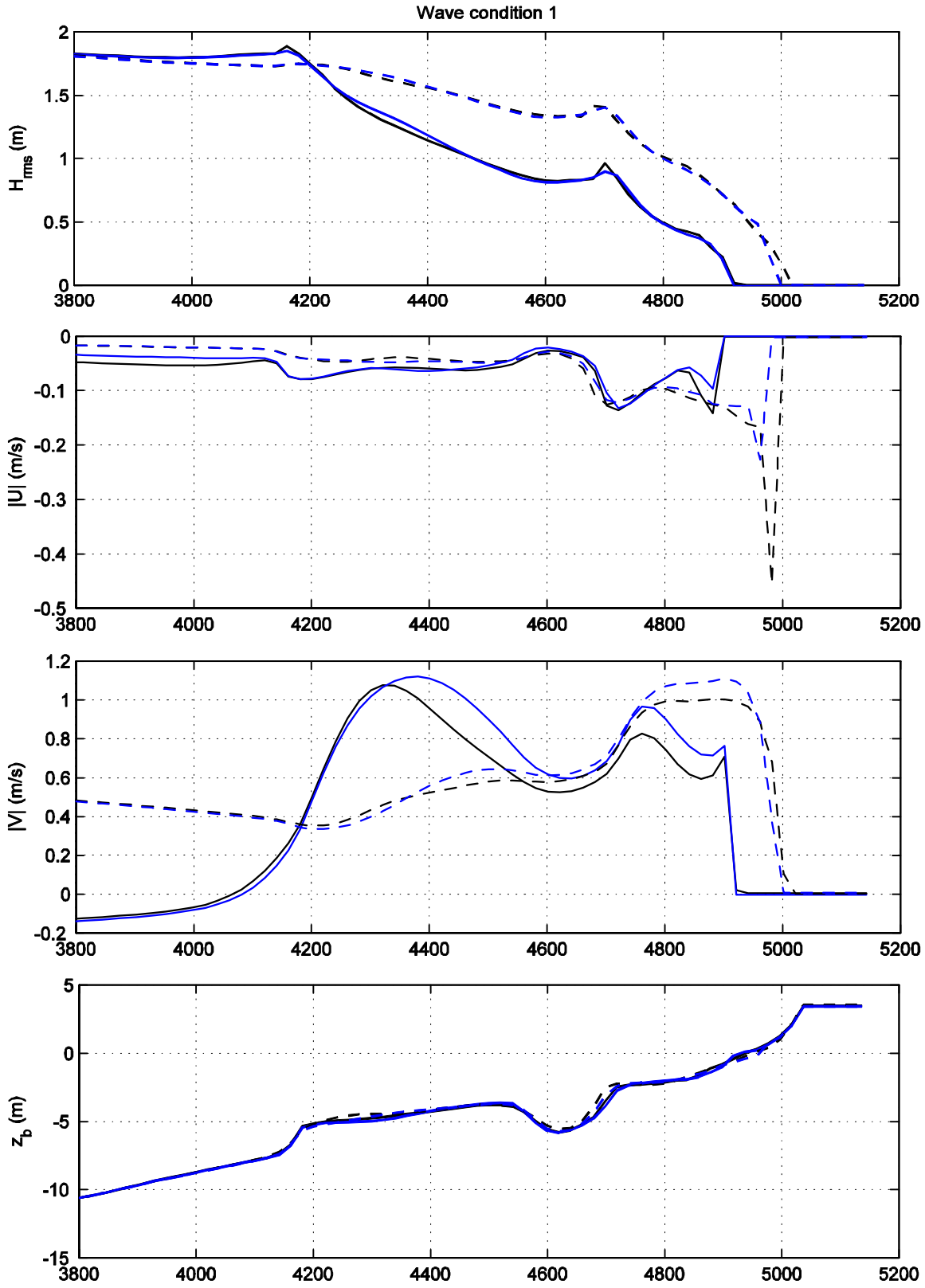

Figure 4.15 *Root-mean-square wave height, depth-averaged cross-shore and longshore current velocity and bed level along the central cross-shore transect. Black lines: standard Delft3D version, blue lines: adjusted Delft3D version, solid lines: at low tide, dashed lines: at high tide.*

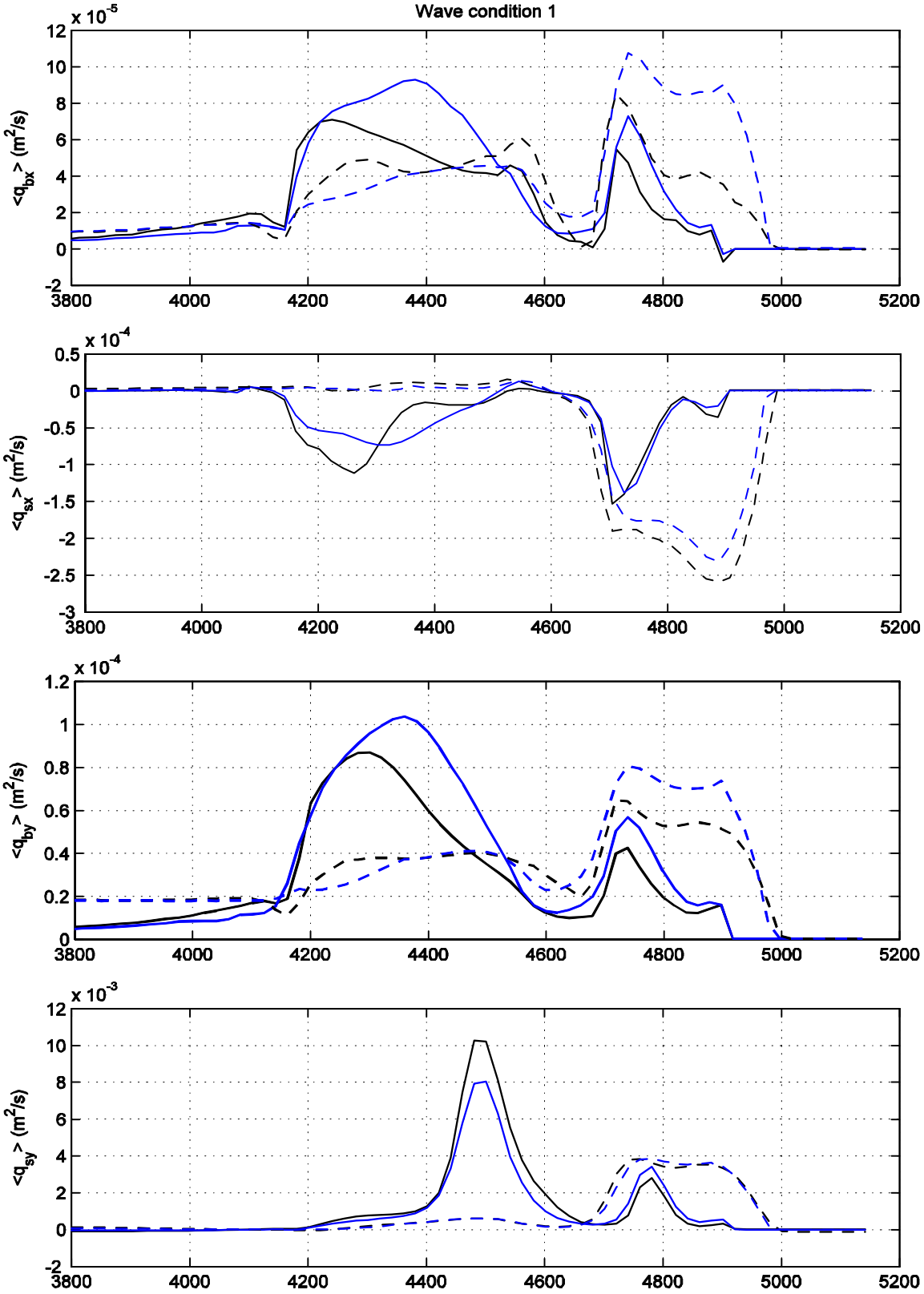

Figure 4.16 *Cross-shore and longshore bedload and suspended load along the central cross-shore transect. Black lines: standard Delft3D version, blue lines: adjusted Delft3D version, solid lines: at low tide, dashed lines: at high tide.*

From Figure 4.15 the following observations can be drawn:

- Longshore currents are higher in the modified Delft3D. This is mainly related to a different method for calculating the shear stresses (Section 2.7).
- Offshore directed cross-shore currents are slightly lower in the modified Delft-3D version, leading to a lower offshore migration of the bar.

In Figure 4.16 the cross-shore and longshore transports as computed by the standard and modified Delft3D for the nourished case were intercompared. The Figure shows that:

- The cross-shore bedload component is onshore directed for both the standard and modified Delft3D versions. This is explained by the fact that wave asymmetry is the dominant process leading to a net onshore transport. This component is enhanced in the modified Delft 3D version.
- The cross-shore suspended load component, calculated by the standard Delft3D version, shows a higher peak offshore the outer bar. In the modified version, the peak in offshore transport is reduced and the transport is more uniform. This might be related to the different advection scheme for suspended sediment transport.
- Longshore bedload and suspended load transports are higher in the modified than in the standard Delft3D version. This behaviour is essential due to the different way of calculating the shear stresses.

5 Conclusions and recommendations

5.1 Conclusions

Based on the results presented in this report we conclude the followings:

- The formation of quasi-rhythmic bottom features along the coastline, despite being a process, which is observed in reality, is exaggerated by simulations run with the standard Delft3D code. The strong feedback between hydrodynamics and morphodynamics leads to an uncontrolled growth of bedforms which does not allow running long term morphodynamics simulation. This behaviour is evident especially for waves approaching nearly perpendicularly the coast.
- The following modifications were included in the standard Delft3D code:
  - Modification of the shear stress calculation by using velocities at the top of the wave boundary layer instead of at the bottom layer.
  - Calculation of the suspended sediment transport by means of a first order upwind scheme, in place of a third order upwind scheme.
  - Correction to the transport routines in order to fix errors in the sediment mass balance.
  - Changes to the roller model routines when this is used in combination with hard structures.
  - Implementation of the quasi-3D approach.
  - Implementation of a module for beach and dune erosion and growth.

  In particular, the first two modifications were investigated extensively in this report.
- Main result of the modifications to the standard Delft3D code is a large increase of the longshore velocities mainly due to the different approach of calculating the shear stress. As a consequence, the longshore sediment transport component is subjected to a relative increse.
- In terms of morphodynamic changes, the increase in longshore transport leads to a smoothing of the quasi-rhythmic bottom features leading to more realistic results.
- The model captures the offshore bar migration during high wave events and the onshore bar migration during low wave events. However, the considerable bar flattening after 1 year of computation is not realistic.
- Both model versions compute an unrealistically high erosion of the inter-tidal area.
- The two model versions compute a qualitatively similar impact of the shoreface nourishment on the nearshore morphology.
- The nourishment diffuses with almost no longshore migration. The coastal area shoreward of the nourishment benefits mostly of its presence. This is due to the so-called lee and feeder effects.
- In line with field observations, the computations show that the nourishment and the original outer bar merge into a new outer bar and that the migration direction of the inner bar reverses from off- to onshore. However, in contrary to field observations the offshore migration of the outer bar is not halted. Furthermore, the inner bar flattens so much that it can hardly be identified as a bar. This might be the result of too large values for the longitudinal and transversal bedload tuning parameter (Alfabn and Alfabs).

- A larger amount of sand accumulates shoreward of the nourishment for simulations run with the modified Delft3d version, while more sand is eroded in the areas seaward, northward and southward of the nourishment. This is related to a increase of the onshore sediment transport component and of the longshore components.
- One simple test with the dune module has shown its capabilities to represent changes in dune position in function of changes in beach width.

5.2 Recommendations

Based on this conclusion we give the following suggestions for further work:

- The modified version of the Delft3D code appears to give a better representation of the morphodynamic processes with respect to the standard Delft3D version. However, further validation based on hydrodynamics measurements and bathymetry surveys is necessary in order to draw final conclusions. These validations tests should also include long term morphodynamic calculations (time scale of years).
- The breakers bars are flattened exceptionally during the simulations. Further investigation is needed in order to get more insight into this process. In particular, a better representation of some hydrodyanamics processes (e.g. correction of the mass balance to compensate roller forces) might be relevant for solving this question. The use of a different numerical scheme for bedload transport (central in place of upwind) might also help reducing this flattening.
- Further investigation is necessary in order to understand the mechanisms leading to the high erosion in the intertidal areas. Additional adjustments to the code are required in order to better represent the physics inside this area. Moreover, the use of different grain distribution along the cross shore profile might help to have a better morphodynamic representation and reduce the erosion of this area.
- The approach of waves, under specific wave angles, induce the formation of quasi-rhythmic features at the bottom. The wave length of these features is related to the specific wave condition. Numerical simulations have shown that the amplitude of these bedforms is exaggerated by the model. This effect might be related to the fact that only few wave conditions have been selected, leading to the exaggerated growing of specific bedform wavelengths. Further investigation is necessary in order to assess the behaviour of these bedforms when more wave conditions are used. Moreover, the effect of parallel on-line runs (“mormerge” procedure), where different wave conditions are run at the same time on different processors and the morphodynamics results merged after each time step should be assessed. Finally, results should be compared with a computation run with the complete wave and tide time series, in order to avoid forcing of some specific bedform wave lengths related to some specific wave angles.
- One nourishment scenario was implemented within this report. However, the design of different nourishment methodologies is regularly asked by the Minister of Transport, Public Works, and Water Management (Rijkswaterstaat). Further work will include the testing of different nourishment geometries, also varying the grain size of the material put into place.
- The impact of the nourishment should be expressed in terms of management parameters (e.g. MKL position), in order to be able to quantify the nourishment efficiency.
- The quasi-3D routines should be validated in further studies. This could provide the possibility of running morphological studies in the nearshore area where the

vertical velocity profile differs from the logarithmic one, with computational times comparable to the 2D approach.

- The beach and dune module should be further tested against field measurement, also for long term simulations.

6 References

Arcilla, A.S., Roelvink, J.A., O'Connor, B., Reniers, A., Jimenez, J.A., 1994. *The Delta flume '93 experiment.* Proceedings Coastal Dynamics Conference, Barcelona, Spain.

Baptist, M.J., Tamis, J.E., Borsje, B.W., Van der Werf, J.J., 2009. *Review of the ecological and biogeomorphological effects of shoreface and beach nourishments on the Dutch sandy coast*. Report (In press), Imares, The Netherlands.

Battjes, J.A., Janssen, J.P.F.M., 1978. *Energy loss and set-up due to breaking of random waves.* Proceedings of the 16th International Conference of Coastal Engineering, 569-587.

Castelle, B., Bonneton, P., Butel, R., Dupuis, H., 2005. *Morphodynamic modeling of nearshore crescentic bar dissymmetry on an open coast: Aquitanian coast, France.* 5th International Conference of Coastal Dynamics 2005, Barcelona, Spain, 11 pp.

Castelle, B., Bonneton, P., Butel, R., 2006. *Modelisation du festonnage des barres sableuses d'avant-côte: application à la côte Aquitaine, France.* Journal of Comptes Rendus Geosciences, 338, 795 – 801.

Cohen, A.B., Brière, C., 2007. Evaluatie van de uitgevoerde suppleties bij Egmond op basis van Argus video waarnemingen, WL|Delft Hydraulics report Z4212, the Netherlands (In Dutch).

De Vriend and Roelvink, 1998. De Vriend H.J. en Roelvink J.A. ,1989. Innovatie van kustverdediging: inspelen op het kustsysteem. Kustverdediging na 1990, technisch rapport 19. WL | Delft Hydraulics rapport H825.

Elias, E.P.L., Walstra, D.J.R., Roelvink, J.A., Stive, M.J.F., Klein, M.D., 2000. *Hydrodynamic validation of Delft3D with field measurements at Egmond.* In: Edge, B.L. (Ed.), Proc. 27th Int. Conf. on Coastal Engineering. ASCE, New York, pp. 2714–2727.

Falqués, A., Montoto, A., Iranzo, V., 1996. *Bed-flow instability of the longshore current.* Journal of Continental Shelf Research, Vol.16, No. 15, 1927-1964.

Falqués, A., Dodd, N., Garnier, R., Ribas, F., MacHardy, L.C., Larroudé, P., Calvete, D., Sancho, F., 2008. Rhythmic surf zone bars and morphodynamic self-organization. Journal of Coastal Engineering, 55, 622-641.

Fredsøe, J., 1984. *Turbulent boundary layer in wave-current motion*. Journal of Hydraulic Engineering, ASCE, 110, 1103-1120.

Grunnet, N.M., Walstra, D.J.R., Ruessink, B.G., 2004. Process-based modeling of a shoreface nourishment, Coastal Engineering, 51: 581-607.

Hasselmann, K., Barnett, T.P., Bouws, E., Carlson, H., Cartwright, D.E., Enke, K., Ewing, J.A., Gienapp, H., Hasselmann, D.E., Kruseman, P., Meerburg, A., Muller, A., Olbers, D.J., Richter, K., Sell, W., Walden, H, 1973. *Measurements of wind-wave growth and swell decay during the Joint North Sea Wave Project (JONSWAP).* Technical report, Hamburg, Germany, A8 (12), 1973.

Henrotte, J., 2008. *Implementation, validation and evaluation of a Quasi-3D model in Delft3D.* Master thesis, Technical University of Delft, The Netherlands.

Hoekstra, P., Houwman, K.T., Kroon, A., Ruessink, B.G., 1996. Morphodynamic behaviour of the Terschelling shoreface nourishment, NOURTEC report, University of Utrecht, The Netherlands.

Kroon, A., Hoekstra, P., Ruessink, G., 1994. Morphological monitoring of a shoreface nourishment NOURTEC experiment at Terschelling, The Netherlands, Proceedings International Conference on Coastal Engineering, Kobe, Japan, pp. 2222-2236.

Latteux, B., 1995. *Techniques for long-term morphological simulation under tidal action*. Journal of Marine Geology, 126, 129 – 141.

Lesser,G.R., Roelvink, J.A., van Kester, J.A.T.M., Stelling, G.S., 2004. *Development and validation of a three dimensional morphological model.* Journal of Coastal Engineering, 51, 883-915.

MacMahan, J.H., Thornton, Ed B., Reniers Ad J.H.M., 2006. *Rip current review*. Journal of Coastal Engineering, 53, 191 – 208.

Munk, W.H., 1949. *The solitary wave theory and application to surf problems*. Ann. N.Y. Acad. Sci. 51 (3), 376-424.

Ojeda, E., Ruessink, B.G., Guillen, J., in press. Morphodynamic response of a two-barred beach to a shoreface nourishment, Coastal Engineering.

Reniers, A., and Battjes, J.A., 1997. *A laboratory study of longshore currents over barred and non-barred beaches.* Coastal Engineering, 30(1-2): 1-21.

Reniers, A.J.H.M., Roelvink, J.A., Thornton, E.B., 2004. *Morphodynamic modeling of an embayed beach under wave group forcing.* Journal of Geophysical Research, 109.

Roelvink, J.A. 1993. *Dissipation in random wave groups incident on a beach,* Journal of Coastal Engineering, 19, 127 – 150.

Roelvink, J.A., Meijer, T.J.G.P., Houwman, K., Bakker, R., Spanhoff ,R., 1995. *Field validation and application of a coastal profile model.* In: Dally, W.R., Zeidler, R.B. (Eds.), Proc. 2nd Int. Conf. on Coastal Dynamics '95. ASCE, New York, 818–828.

Roelvink, J.A., 1999. *Kleinschalig Morfologisch Onderzoek MV2*, WL | Delft Hydraulics report Z2627_1B.

Roelvink, J.A., Walstra, D.J.R., 2004. *Keeping it simple by using complex models.* Int. Conf. on Hydroscience and Engineering (ICHE-2004), Brisbane, Australia.

Ruessink, B.G., Walstra, D.J.R., Southgate, H.N., 2003. *Calibration and verification of a parametric wave model on barred beaches.* Journal of Coastal Engineering, 48, 139 – 149

Short, A.D., 1992. *Beach systems of the central Netherlands coast: Processes, morphology and structural impacts in a storm driven multi-bar system.* Journal of Marine Geology, 107, 103 – 137.

Treffers, R., 2009. *Wave-Driven Longshore Currents in the Surf Zone. Hydrodynamic validation of Delft3D. Master thesis,* Technical University of Delft, The Netherlands.

Van Duin, M.J.P., 2002. *Evaluation of the Egmond shoreface nourishment : part III : validation morphological modelling Delft3D-MOR,* WL | Delft Hydraulics report Z3054/Z3148.

Van Duin, M.J.P., Wiersma, N.R., Walstra, D.J.R., Van Rijn, L.C., Stive, M.J.F., 2004. *Nourishing the shoreface: observations and hindcasting of the Egmond case, The Netherlands.* Journal of Coastal Engineering, 51: 813-837.

Van Rijn L.C., 2007a. *Unified view of sediment transport by currents and waves. I: Initiation of motion, bed roughness, and bed-load transport.* Journal of Hydraulic Engineering-ASCE 133 (6): 649-667.

Van Rijn L.C., 2007b. *Unified view of sediment transport by currents and waves. II: Suspended transport.* Journal of Hydraulic Engineering-ASCE 133 (6): 668-689.

Van Rijn, L.C., 2007c. Unified view of sediment transport by currents and waves. III: Graded beds. Journal of Hydraulic Engineering, 133: 761-775.

Walstra, D.J.R., Van Ormondt, M., Roelvink, J.A., 2004. *Shoreface Nourishment Scenarios,* WL | Delft Hydraulics report Z3748.21.

Walstra, D.J.R., Brière C., Cohen, A.B., van Dongheren, A.P., Elshoff, I.J.P., Hoying, C., van Ormondt, M., Quartel, S., de Sonneville, B., Tonnon, P.K., Uunk, L., **2008.** *Monitoring and Modelling of a shoreface nourishment,* WL | Delft Hydraulics report Z4479.

7 Appendix A

The following steering files refer to the schematized Egmond case for runs with the standard version of the code. For runs with the modified version add the following keywords:

In the MDF file:

Wbndly= -1 # Shear stress calculated using the velocity at the top of the wave boundary layer

In the MOR file:

FirstOrderUpwind = true

7.1 Master Definition Flow File (MDF file)

```
Ident = #Delft3D-FLOW  .03.02 3.39.09#
Runid = #prf#
Commnt=
Filcco= #2d_ext.grd#
Fmtcco= #FR#
Anglat=  5.5000000e+001
Grdang=  0.0000000e+000
Filgrd= #2d.enc#
Fmtgrd= #FR#
MNKmax= 71 137 12
Thick =  2.0000
         3.2000
         5.0000
         7.9000
        12.4000
        19.6000
        19.6000
        12.4000
         7.9000
         5.0000
         3.2000
         1.8000
Fildep= #profile.dep#
Fmtdep= #FR#
Commnt=
MNdry = [ ] [ ] [ ] [ ]
Fildry= ##
Fmtdry= #FR#
```

```
MNtd  = [ ] [ ] [ ] [ ] #U#
Filtd = ##
Fmttd = #FR#
Nambar= #                #
MNbar = [ ] [ ] # #
MNwlos= [ ] [ ]
Commnt=
Itdate= #2004-01-01#
Tunit = #M#
Tstart=  240.0
Tstop =  1230.0
Dt    =  2.0000000e-001
Tzone = 0
Commnt=
Sub1  = #    #
Sub2  = # CW#
Namc1 = #Sediment sand      #
Namc2 = #                #
Namc3 = #                #
Namc4 = #                #
Namc5 = #                #
Wnsvwp= #N#
Filwnd= ##
Fmtwnd= #FR#
Wndint= #Y#
Commnt=
Filic = ##
Zeta0 = 1.05
U0    = [.]
V0    = [.]
S0    = [.]
T0    = [.]
C01   =  0.0000000e+000
         0.0000000e+000
         0.0000000e+000
         0.0000000e+000
         0.0000000e+000
         0.0000000e+000
         0.0000000e+000
         0.0000000e+000
         0.0000000e+000
         0.0000000e+000
         0.0000000e+000
         0.0000000e+000
```

```
      0.0000000e+000
Restid= ##
Commnt=
Filbnd= #profile.bnd#
Fmtbnd= #FR#
FilbcH= #090104n.bch#
FmtbcH= #FR#
FilbcT= ##
FmtbcT= #FR#
FilbcQ= ##
FmtbcQ= #FR#
Filana= ##
Filcor= ##
FilbcC= #2dh.bcc#
FmtbcC= #FR#
Rettis=  0.0000000e+000
      0.0000000e+000
      0.0000000e+000
Rettib=  0.0000000e+000
      0.0000000e+000
      0.0000000e+000
Commnt=
Ag    =  9.8100004e+000
Rhow  =  1.0230000e+003
Alph0 = [.]
Tempw =  1.0000000e+001
Salw  =  3.1000000e+001
Rouwav= #FR84#
Wstres=  6.3000002e-004  0.0000000e+000  7.2300001e-003  1.0000000e+002
Rhoa  =  1.0000000e+000
Betac =  5.0000000e-001
Equili= #N#
Tkemod= #K-epsilon   #
Ktemp = 0
Fclou =  0.0000000e+000
Sarea =  0.0000000e+000
Filtmp= ##
Fmttmp= #FR#
Temint= #Y#
Tstmp = [.] [.]
Commnt=
Roumet= #C#
Filrgh= ##
```

Ccofu = 6.5000000e+001
Ccofv = 6.5000000e+001
Xlo = 0.0000000e+000
Filedy= ##
Vicouv= 1.0000000e-000
Dicouv= 1.0000000e-000
Vicoww= 1.0000000e-006
Dicoww= 1.0000000e-006
Irov = 0
Z0v = [.]
Cmu = [.]
Cpran = [.]
Filsed= #profile.sed#
Filmor= #profile.mor#
Commnt=
Iter = 2
Dryflp= #YES#
Dpuopt= #MOR#
Dpsopt= #DP#
Dryflc= 2.0000000e-001
Dco = 1.0000000e+000
Tlfsmo= 3.0000000e+001
ThetQH= 0.0000000e+000
Forfuv= #Y#
Forfww= #N#
Sigcor= #N#
Trasol= #Cyclic-method#
Commnt=
Filsrc= ##
Fmtsrc= #FR#
Fildis= ##
Fmtdis= #FR#
Commnt= no. observation points: 0
Filsta= #profile.obs#
Fmtsta= #FR#
Tpar = [.] [.]
XYpar = [.] [.]
Commnt=
Eps = [.]
Commnt=
Commnt= no. cross sections: 0
Namcrs= # #
MNcrs = [ ] [ ] [ ] [ ]

```
Commnt=
SMhydr= #YYYYY#
SMderv= #YYYYYY#
SMproc= #YYYYYYYYYY#
PMhydr= #YYYYYY#
PMderv= #YYY#
PMproc= #YYYYYYYYYY#
SHhydr= #YYYY#
SHderv= #YYYYY#
SHproc= #YYYYYYYYY#
SHflux= #YYYY#
PHhydr= #YYYYYY#
PHderv= #YYY#
PHproc= #YYYYYYYYY#
PHflux= #YYYY#
Commnt=                         attribute file fourier analyzed
Filfou= ##
Online= #NO #
Prmap = [.]
Prhis = [.] [.] [.]
Flmap =  480.0000000e+000  30.  1230.
Flhis =  0.0000000e+000  1.0000000e+001  1230.0
Flpp  =  0.0000000e+000  1.0000000e+001  1230
Flrst =  0.0000000e+000
Commnt=
Bndneu= #YES#
Cstbnd= #YES#
Roller= #YES#
Snelli= #NO#
Gamdis= -1
betaro= 0.05
F_lam = -2.0
TraFrm= #vrijn2004.frm#
Trtrou= #N#
Trtdef= #vrijn04.trt#
Trtu  = #trtuv.inp#
Trtv  = #trtuv.inp#
TrtDt = 2.
Waveol= #YES#
Commnt=
```

7.2 Master Definition Wave File (MDW file)

```
Delft3D WAVE GUI version 4.88.01
'40.01'
* Project name, -number
''
''
* Description
''
''
''
* Y/N Use bathmetry, use waterlevel, use current
1 1 1
* Number of computational grids
1
* Filename comp. grid
'wave_ext.grd'
* Y/N bathymetry is based on comp. grid, filename bath. grid
1 ''
* Filename bathymetry data
'wave_ext.dep'
* Directional space: type, number of directions,
*                   start-direction, end-direction
*   - type: 1 = circle, 2 = sector
2 18  1.8000000e+002  0.0000000e+000
* Frequency space: lowest frequency, highest frequency, number of freq. bins,
*                  grid to nest in, Y/N write output for this grid
 5.0000001e-002  1.0000000e+000 24 0 1
* Number of tidal time points
1
* Time, h, u, v
 0.0000000e+000 -9.9900000e+002 -9.9900000e+002 -9.9900000e+002
* Waterlevel correction
 0.0000000e+000
* Number of boundaries
3
* Boundary name, specifications, defined-by, conditions-along-boundary
*   - specifications: 1 = from-file, 2 = parametric
*   - defined-by: 1 = orientation,
*                 2 = grid-coordinates,
*                 3 = xy-coordinates
*   - conditions-along-boundary: 1 = constant, 2 = variable
'Boundary 1' 2 1 1
```

```
* Orientation
*   1 = N, 2 = NW, 3 = W, 4 = SW, 5 = S, 6 = SE, 7 = E, 8 = NE
1
* Shape, period, width-energy, peak enhancement factor, spreading
*   - shape: 1 = Jonswap, 2 = Pierson-Moskowitz, 3 = Gauss
*   - period: 1 = Peak, 2 = Mean
*   - width-energy: 1 = Power, 2 = Degrees
1 1 1 3.300000 0.010000
* Significant waveheight, peak period, direction, energy distribution
 0.0000000e+000  0.0000000e+000  0.0000000e+000  0.0000000e+000
* Boundary name, specifications, defined-by, conditions-along-boundary
*   - specifications: 1 = from-file, 2 = parametric
*   - defined-by: 1 = orientation,
*                 2 = grid-coordinates,
*                 3 = xy-coordinates
*   - conditions-along-boundary: 1 = constant, 2 = variable
'Boundary 2' 2 1 1
* Orientation
*   1 = N, 2 = NW, 3 = W, 4 = SW, 5 = S, 6 = SE, 7 = E, 8 = NE
3
* Shape, period, width-energy, peak enhancement factor, spreading
*   - shape: 1 = Jonswap, 2 = Pierson-Moskowitz, 3 = Gauss
*   - period: 1 = Peak, 2 = Mean
*   - width-energy: 1 = Power, 2 = Degrees
1 1 1 3.300000 0.010000
* Significant waveheight, peak period, direction, energy distribution
 0.0000000e+000  0.0000000e+000  0.0000000e+000  0.0000000e+000
* Boundary name, specifications, defined-by, conditions-along-boundary
*   - specifications: 1 = from-file, 2 = parametric
*   - defined-by: 1 = orientation,
*                 2 = grid-coordinates,
*                 3 = xy-coordinates
*   - conditions-along-boundary: 1 = constant, 2 = variable
'Boundary 3' 2 1 1
* Orientation
*   1 = N, 2 = NW, 3 = W, 4 = SW, 5 = S, 6 = SE, 7 = E, 8 = NE
5
* Shape, period, width-energy, peak enhancement factor, spreading
*   - shape: 1 = Jonswap, 2 = Pierson-Moskowitz, 3 = Gauss
*   - period: 1 = Peak, 2 = Mean
*   - width-energy: 1 = Power, 2 = Degrees
1 1 1 3.300000 0.010000
* Significant waveheight, peak period, direction, energy distribution
```

```
 0.0000000e+000  0.0000000e+000  0.0000000e+000  0.0000000e+000
* Number of obstacles
0
* Gravity, water density, north, minimum depth
 9.8100004e+000  1.0250000e+003  9.0000000e+001  5.0000001e-002
* Convention, setup, forces
*   - convention: 1 = nautical, 2 = cartesian
*   - setup: 0 = no setup, 1 = activated
*   - forces: 1 = radiation stress, 2 = wave energy dissipation rate
1 0 2
* Wind type (1 = constant, 2 = variable)
1
* Wind speed, -direction
 0.0000000e+000  0.0000000e+000
* Type of formulations
*   0 = none, 1 = 1-st, 2 = 2-nd, 3 = 3-th generation
3
* Depth induced breaking, alpha, gamma
*   - breaking: 0 = de-activated, 1 = B&J model
1  1.0000000e+000  7.3000002e-001
* Bottom friction, friction coefficient
*   - friction: 0 = de-activated, 1 = Jonswap,
*               2 = Collins, 3 = Madsen et al.
1  6.7000002e-002
* Non-linear triad interactions, alpha, beta
*   - interactions: 0 = de-activated, 1 = LTA
0  1.0000000e-001  2.2000000e+000
* Y/N windgrowth, white-capping, quadruplets, refraction, freq. shift
0 0 0 1 0
* Directional space, freq. space
 5.0000000e-001  5.0000000e-001
* Hs-Tm01, Hs, Tm01, perc. of wed grid points, max. number of iterations
 2.0000000e-002  2.0000000e-002  2.0000000e-002  9.8000000e+001 15
* Number of output curves
0
* Level of test output, debug level, Y/N compute waves
0 0 1
* Y/N output to Flow grid; filename of Flow grid
1 '2d_ext.grd'
* Y/N output to locations
0
```

7.3 Morphology input file (MOR file)

```
[MorphologyFileInformation]
  FileCreatedBy    = Delft3D-FLOW-GUI, Version: 3.1804
  FileCreationDate = 19-12-2003,  8:50:45
  FileVersion      = 02.00
[Morphology]
  MorFac = 10.00       [ - ] Morphological scale factor
  MorStt = 240.      [ - ] Start time for bed updating (in minutes rel. to simulation start time)
  Thresh = 0.2       [ m ] Threshold sediment thickness for reducing sediment exchange
  MorUpd = true      [T/F] Update bathymetry during flow run
  EqmBc  = true      [T/F] Equilibrium concentration at inflow boundaries
  DensIn = false     [T/F] Include effect of sediment on density gradient
  AksFac = 1.0       [ - ] Van Rijn's reference height = AKSFAC * KS
  RWave  = 1.0       [ - ] Wave related roughness = RWAVE * estimated ripple height. Van Rijn Recommends range 1-3
  AlfaBs = 20.0      [ - ] Longitudinal bed gradient factor for bed load transport
  AlfaBn = 20.0      [ - ] Transverse   bed gradient factor for bed load transport
  Sus    = 1.0       [ - ] Suspended transport factor
  Bed    = 1.0       [ - ] Bedload transport factor
  SusW   = 0.5       [ - ] Wave-related suspended transport factor
  BedW   = 1.0       [ - ] Wave-related bedload transport factor
  SedThr = 0.25      [ m ] Minimum depth for sediment computations
  ThetSD = 1.0       [ - ] Fraction of erosion to assign to adjacent dry cells
  FWFac  = 0.0       [ - ] Tuning parameter for wave streaming
  EpsPar = false     [T/F] Only for waves in combination with k-epsilon turbulence model
                     TRUE : Van Rijn's parabolic-linear mixing distribution for current-related mixing
                     FALSE: Vertical sediment mixing values from K-epsilon turbulence model
  IopKCW = 1         [ - ] Flag for determining Rc and Rw (Only for Van Rijn (1993))
                     1 (default): Rc from flow, Rw=RWAVE*0.025
                     2          : Rc=RDC and Rw=RDW as read from this file
                     3          : Rc=Rw determined from mobility
  RDC    = 0.01      [ - ] Rc in case IopKCW = 2
  RDW    = 0.02      [ - ] Rw in case IopKCW = 2
  UpdInf = true      [T/F] Flag for updating bed at inflow boundaries
                     FALSE (default) : Bed level constant
                     TRUE            : Down-wind approach
  CaMax  = 0.05
  DzMax  = 0.05
```

7.4 Sediment file (SED file)

```
[SedimentFileInformation]
  FileCreatedBy    = Delft3D-FLOW-GUI, Version: 3.1804
  FileCreationDate = 19-12-2003,  8:50:45
  FileVersion      = 02.00
[SedimentOverall]
  Cref   = 10.e+5         [kg/m3 ] = CSoil Reference density for hindered settling calculations
  IopSus = 1      [  -   ] 1: Suspended sediment size is calculated dependent hydrodynamic conditions and d50
[Sediment]
  Name   = #sediment sand# [  -   ] Name as specified in NamC in md-file
  SedTyp = sand           [  -   ] Must be "sand" or "mud"
  RhoSol = 2650.0         [kg/m3 ] Density
  SedDia = 0.00020                [  m   ] Sand only: Sediment diameter
  SedD10 = 0.00015                [  m   ] Sand only: Sediment diameter
  SedD90 = 0.00030                [  m   ] Sand only: Sediment diameter
  CDryB  = 1600.0         [kg/m3 ] Dry bed density
  SdBUni = 16000.0       # [kg/m2 ] Initial sediment mass at bed per unit area  (uniform value or file name)
  FacDSS = 1.0      [  -   ] FacDss * SedDia = Initial suspended sediment diameter. range [0.6 - 1.0]
```